One-dimensional modeling of concentration propagation in the human circulatory system

AM3000 TWN: Bachelor Thesis

Author S.H.H. Groen

Instructors C. Vuik and S. Kenjeres
Faculty EEMCS and TNW
(Delft, University of Technology)

Date: June 30, 2023

Abstract

This thesis investigates the behaviour of one-dimensional blood flow in the human arterial tree. It focuses on modeling the change in velocity, cross-sectional area, and concentration. The equations governing this flow are derived using the physical laws of conservation of mass, conservation of momentum, and the advection-diffusion equation. To solve this set of equations numerically, the Finite Volume Method in combination with a flux difference splitting approach is employed.

The study begins with an examination of a single artery, revealing wave-like behavior in pressure and concentration. Pressure propagates along the vessel, while concentration gradually dilutes over time. This behaviour is also visible when expanding to the 55-artery model of the entire human body. The results of this model were found to be very comparable to the literature. Additionally, the propagation of a chemical species injected into an artery near the heart is investigated. It takes around 25 seconds to propagate to the legs but the amount of concentration is greatly reduced. The strength of this wave upon reaching the legs is investigated for different values of the diffusion coefficient. It is found that when $D = 0.02$ cm^2/s, the strength is around the 80% of its original value while a value of $D = 2$ cm^2/s reduces it to 40%. Further research should focus on expanding this model and improving its accuracy. Especially the exact concentration waves in single arteries are very prone to spurious oscillations. By optimizing the numerical code, the accuracy can be greatly increased. Moreover, more realistic additions can be made to this model. Such as expanding to a two-way model enabling to inject at various points around the arterial tree. Nevertheless, this model provides insight into the propagation of blood and concentration in the human circulatory system, highlighting the need for refinement.

Contents

1 Introduction

The year 2020 will forever be remembered as the time when COVID-19 swiftly transformed into a global pandemic, impacting every aspect of our lives. It started as an innocent virus but quickly became a world-dominating disease. As our global population continues to grow at an unprecedented rate, the threat posed by such epidemics becomes increasingly significant. Luckily, scientists have shown themselves capable of developing vaccines to effectively combat these diseases. Upon injecting such a vaccine, the concentration of antigens is not evenly distributed. Instead, it initiates a fascinating process of concentration propagation.

When a concentration is injected into the body, it begins to spread and flow through the arteries, undergoing two important processes: diffusion and advection. Understanding these properties is crucial to understand the behaviour of concentration flow in the human body. However, studying these properties requires knowledge about blood flow, which has historically been challenging. The underlying mechanisms are extremely complex, involving the collaboration of millions of individual components. However, in recent years our ever-growing computation power has come to be very useful. Originally, the 3D blood flow can be described by the Navier-Stokes equations. Unfortunately, the computation complexity of models based on these equations remains high so simplifications must be made. Researchers like Sherwin et al. [1] have shown that one-dimensional blood flow models can greatly reduce computational time while enjoying very realistic results.

In this thesis, we will derive a set of equations to describe the concentration- and blood flow in the human arterial tree. Unfortunately, these equations do not have a closed-form solution so we must rely on numerical approaches. One particularly effective approach is the Finite Volume Method. This method ensures conservation of mass and momentum and proves highly valuable in solving physical problems like this one. With the numerical methods, the set of equations is then tried to be solved. This project then aims to use the numerical solution of the velocity and pressure inside the arteries, to model the propagation of concentration in the body. To that end, the thesis can be divided into two parts. Firstly, we numerically investigate the model recommended by Sherwin et al. [1] and the solutions for the velocity and pressure inside the artery are computed. With this in hand, we proceed to model the concentration propagation. The flow of concentration is described by the advection-diffusion equation which required information about the velocity. With this known, a simulation can be made to understand the propagation of a vaccine injected in the tree. This report will explain the steps taken during this thesis. It starts in chapter 3 by deriving a system of equations that describe the flow of blood and concentration in the circulatory system. In order to effectively implement the numerical methods, the derived system should be rewritten in his *characteristic form*. This is done in chapter 4. In chapter 5 we derive our numerical scheme and test it on a simplified *linear* test function. Since our final system is *nonlinear* the methods from chapter 5 are expanded to nonlinear cases. This is done in chapter 6. In chapters 7 and 8 we test the behaviour of the flow in simple test arteries. In both a normal and a stented artery, the pressure and concentration propagation are analysed. In chapter 9 we determine how to model important features of the human arterial tree. These include for example the bifurcations and the modeling of the heart. With that all done, we are finally in the position to model the entire tree and investigate the propagation of an injected concentration. This is done in chapter 10. This will all lead to answering the following research question: *How does concentration propagate in the human arterial tree?*

2 Literature survey

In this chapter, we give a short description of the current work which has been done on 1D blood flow modeling. In recent years, numerous studies have focused on modeling blood flow in the human arterial tree. These researches involve deriving a system of coupled partial differential equations (PDEs). Conservation laws, which play a crucial role in arterial flow dynamics, are used to derive these PDEs. The conservation of mass leads to an equation based on volumetric flow (Q) and velocity (u), while the conservation of momentum results in an equation based on cross-sectional area (A) and velocity (u). This has been done in studies like [1, 2, 3]. The main difference between these works is their relation between pressure and cross-sectional area. In [4] a list of the different relations can be found. In our work, we will adopt the relation used in, for example, [1, 5].

To solve these PDEs, the most common methods used in the literature are the Finite Element Method (FEM) and the Finite Volume Method (FVM). FVM is particularly useful in our problem as mass and momentum are conservated. In literature, different approaches are used. Sherwin [1] for example uses Discontinuous Galerkin while Mynard [4] uses a Taylor-Galerkin approach. We will use a slightly different approach and use the *flux wave decomposition* method. This is explained in [6] and adapted in [7].

Another important factor in the arterial system is how to model the heart. In our work, we will use a rather simple model of the heart which only models the change of cross-sectional area imposed by a heartbeat as introduced in [1] and adopted in [7, 8]. More sophisticated models of the heart, such as those presented [4] and [2], account for the detailed contraction and relaxation behavior of the different chambers.

Bifurcations are a vital element of the circulatory system. These branching points will be modeled by conserving mass and pressure over these bifurcations. With this approach, a system of equations should be solved using *Newton-Raphson* just as in [7, 4, 5].

We also aim to incorporate concentration in the model. This introduces an extra PDE known as the *advection-diffusion equation*. Concentration propagation has been implemented in [3], where a more complex radial-dependent concentration flow model is considered. However, in our model, we focus solely on the 1D value of concentration at different time and spatial points, without incorporating this radial dependency. Solving this concentration PDE can generally be done using two approaches, the central difference method (CDM) or using an upwind scheme. Both have their stability advantages but in general, CDM is more accurate if the Péclet number (see [9] for information about the Péclet number) is below 2 while upwind is more accurate for Péclet numbers above 2. For that reason, we will determine for each problem which approach would be more accurate depending on the Péclet number. The upwind scheme is introduced in [6] and CDM in [10].

3 Derivation of the model

To fully analyse the behaviour of blood flow in the human body, we need a mathematical model describing the one-dimensional flow in the arterial system. The model should describe the propagation of blood through the system as well as show how concentration diffuses through the arteries. To start, we consider a simple artery illustrated in figure 1 to derive the model. Throughout this work, we will assume that the local curvature of the arteries is very small. In that way, we can approximate the axial direction with the Cartesian coordinate x as seen in figure 1.

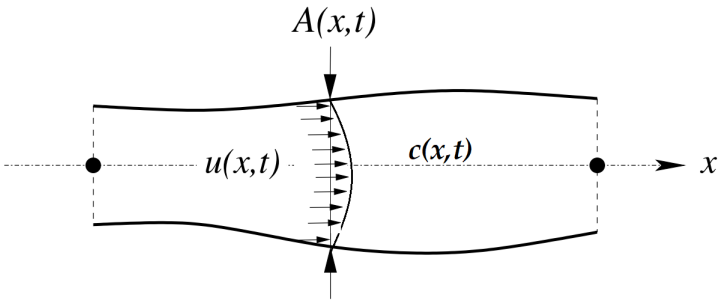

Figure 1: Schematic model of the artery from Peiró et al. [11]. $A(x,t)$ symbolizes the cross-sectional area, $u(x,t)$ the velocity and $c(x,t)$ the concentration at a specific place and time.

We assume the arteries have flexible walls and a fully circular cross area. The cross-sectional area is thus location and time-dependent and denoted by $A(x,t)$. Throughout the thesis, we differentiate between the average velocity denoted by $U(x,t)$ and the axial velocity profile $u(x,\xi,t)$. ξ is the radial coordinate. The axial velocity is assumed to be time-independent. We follow Svitenkov et al. [3] and assume:

$$u(x,\xi,t) = U(x,t)g(\xi) = U(x,t)\frac{\zeta+2}{\zeta}\left(1-\left(\frac{\xi}{R}\right)^{\zeta}\right) \tag{1}$$

Here, $R(x,t)$ is the artery's radius, and ζ is a constant for a particular flow. $\zeta = 9$ is seen as a good approximation for flow in many arteries [12]. So we use that value of ζ. This radial dependency will especially be used when considering friction. Moreover, inside the artery, we introduce some concentration $c(x,t)$ of a chemical species but such, that it does not influence the fluid dynamics. With this set, we are now in the position to derive a system of equations describing the blood and concentration flow through the circulatory system. We will do this by using the conservation laws.

3.1 Conservation of mass

The first conservation law we consider is the conservation of mass. One can understand, that since we assume no mass is being produced inside an artery, the total mass flowing into the artery must equal the total mass flowing out of the artery. As a control volume, we consider an artery with boundaries at $x = a$ and $x = b$. The total mass inside this volume is given by $M = \int_a^b \rho(x,t)A(x,t)dx$, with $A(x,t)$ and $\rho(x,t)$ is the cross area and the density at position x and time t respectively. In this work, we will assume the fluid to be incompressible and hence $\rho(x,t) \equiv \rho$ so independent of time and space. As mentioned above we assume no mass is being produced inside the artery, hence the total mass can only change due to the inflow and outflow of mass. The inflow and outflow rates are known as mass flux and describe

the mass change per unit of time. The mass flux at $x = a$ is given by $\rho A(a,t)U(a,t)$ with $U(a,t)$ the average flow velocity at the boundary. Similarly, the mass flux at $x = b$ can be defined. When combining everything, the change of mass in our control volume can be described as

$$\frac{\partial}{\partial t}\int_a^b \rho A(x,t)dx = \rho A(a,t)U(a,t) - \rho A(b,t)U(b,t) \tag{2}$$

We assume the functions to be sufficiently smooth so we can interchange integral and derivative (please see [13] for the exact conditions). Then we can apply the Fundamental Theorem of Calculus (FTC) on the right-hand side. Note that we get

$$\rho A(a,t)U(a,t) - \rho A(b,t)U(b,t) = -\rho\int_a^b \frac{\partial(AU)}{\partial x}dx \tag{3}$$

Then combining eqn (2) with eqn (3) we get

$$\frac{\partial}{\partial t}\int_a^b \rho A(x,t)dx + \rho\int_a^b \frac{\partial(AU)}{\partial x}dx = \rho\int_a^b \left[\frac{\partial A}{\partial t} + \frac{\partial(AU)}{\partial x}\right]dx = 0 \tag{4}$$

For the integral to equal 0 for any a and b we must have that

$$\frac{\partial A}{\partial t} + \frac{\partial(AU)}{\partial x} = 0 \tag{5}$$

This is our first equation describing the flow in the human circulatory system.

3.2 Conservation of momentum

The next conservation law we use for the derivation of the model is the conservation of momentum. Again we consider as a control volume an artery with boundaries at $x = a$ and $x = b$. The total momentum inside this volume is given by $\int_a^b \rho A(x,t)U(x,t)dx$. The first way in which the momentum of the control volume can change is due to the inflow and outflow of momentum at the boundaries. The momentum flux at the boundaries is given by $\rho A(a,t)U(a,t)^2$ and $\rho A(b,t)U(b,t)^2$. Unlike with mass, momentum can be produced in the control volume by applying a force F. With this, the change of momentum is given by

$$\frac{\partial}{\partial t}\int_a^b \rho A(x,t)U(x,t)dx = \rho A(a,t)U(a,t)^2 - \rho A(b,t)U(b,t)^2 + F \tag{6}$$

To define the applied forces F we will consider viscous and pressure force contributions as done by Sherwin et al. [1]. Then $p(a,t)A(a,t)$ and $p(b,t)A(b,t)$ are the pressure forces acting on the volume at the boundaries, with $p(x,t)$ being the pressure at location x and time t. Next, the contribution of the pressure force on the side walls is given by $\int_a^b p\frac{\partial A}{\partial x}dx$. Lastly, the contribution of the viscous resisting force is given as $\int_a^b f dx$ in which f represents the friction force per unit length. So eqn (6) becomes

$$\frac{\partial}{\partial t}\int_a^b \rho AU dx = \rho A(a,t)U(a,t)^2 - \rho A(b,t)U(b,t)^2 + \int_a^b p\frac{\partial A}{\partial x}dx + \int_a^b f dx + p(a,t)A(a,t) - p(b,t)A(b,t) \tag{7}$$

We again assume we are allowed to rewrite it as

$$\rho\int_a^b \frac{\partial(AU)}{\partial t}dx = -\rho\int_a^b \frac{\partial(AU^2)}{\partial x}dx + \int_a^b p\frac{\partial A}{\partial x}dx + \int_a^b f dx - \int_a^b \frac{\partial(pA)}{\partial x}dx \tag{8}$$

This can be rewritten as

$$\rho \int_a^b \left[\frac{\partial(AU)}{\partial t} + \frac{\partial(AU^2)}{\partial x} - \frac{p}{\rho}\frac{\partial A}{\partial x} - \frac{f}{\rho} + \frac{\partial(pA)}{\partial x} \right] dx = 0 \tag{9}$$

Because the integral is 0 for any a and b we must have that the integrand is 0 so

$$\frac{\partial(AU)}{\partial t} + \frac{\partial(AU^2)}{\partial x} - \frac{p}{\rho}\frac{\partial A}{\partial x} - \frac{f}{\rho} + \frac{\partial(pA)}{\partial x} = 0 \tag{10}$$

Next, we will use the product rule of differentiation to simplify this equation

$$\begin{aligned} \frac{\partial(AU)}{\partial t} &= \frac{\partial A}{\partial t}U + \frac{\partial U}{\partial t}A \\ \frac{\partial(AU^2)}{\partial x} &= \frac{\partial(AU)}{\partial x}U + \frac{\partial U}{\partial x}AU \\ \frac{\partial(pA)}{\partial x} &= \frac{\partial p}{\partial x}A + \frac{\partial A}{\partial x}p \end{aligned} \tag{11}$$

Substituting eqn (11) into eqn (10) we will get

$$A\left[\frac{\partial U}{\partial t} + U\frac{\partial U}{\partial x} + \frac{1}{\rho}\frac{\partial p}{\partial x} - \frac{f}{\rho A} \right] + U\left[\frac{\partial A}{\partial t} + \frac{\partial(AU)}{\partial x} \right] = 0 \tag{12}$$

We note that the terms in the right bracket equal zero by conservation of mass. Moreover, we have assumed an asymmetrical velocity profile described by eqn (1). This means we have a certain viscous friction term $f = -2(\zeta + 2)\nu\pi UA$ [3]. Here ζ is a constant depending on the velocity profile and ν is the kinematic viscosity of blood. Together the second equation describing the flow in the human circulatory system is given by

$$\frac{\partial U}{\partial t} + U\frac{\partial U}{\partial x} + \frac{1}{\rho}\frac{\partial p}{\partial x} + \frac{2}{\rho}(\zeta + 2)\nu\pi U = 0 \tag{13}$$

3.3 Pressure relation

Eqn (5) and (13) can almost be used to describe the blood flow. To complete the system we need an expression for the pressure in terms of U or A. For this, we follow Sherwin et al. [1] and assume

$$p(x,t) = p_{ext}(x,t) + \beta(\sqrt{A(x,t)} - \sqrt{A_0(x,t)}) \tag{14}$$

p_{ext} is the external pressure, A_0 is the equilibrium cross area and β is a measure for the vessel's stiffness given by

$$\beta = \frac{\sqrt{\pi}h_0 E}{(1-\mu^2)A_0} \tag{15}$$

Here h_0 is the thickness of the vessel's wall, $E(x)$ is the Young modules, and μ is the Poisson ratio and commonly set to $\frac{1}{2}$ for tissues.

3.4 Concentration

Combining 5, 13 and 14 allows us to describe the blood flow in the human circulatory system. In this work, we also want to study the propagation of a chemical species through the system. For that, we use the standard advection-diffusion equation

$$\frac{\partial c(x,t)}{\partial t} + U(x,t)\frac{\partial c(x,t)}{\partial x} = D\frac{\partial^2 c(x,t)}{\partial x^2} \tag{16}$$

Where we have assumed that the diffusion coefficient $D(x,t) \equiv D$. The part $U(x,t)\dfrac{\partial c(x,t)}{\partial x}$ describes the advection and $D\dfrac{\partial^2 c(x,t)}{\partial x^2}$ the diffusion part of the PDE. Unlike the velocity, we assume the cross-sectional distribution of agent concentration to be uniform. This will simplify the calculations as it now turns to a convectional transport with $U(x,t)$. For an analysis with more sophisticated concentration profiles, we refer to [3].

4 Characteristic system

In the previous chapter, we have derived a system of non-linear partial differential equations (PDE)

$$\begin{cases} \dfrac{\partial A}{\partial t} + \dfrac{\partial (AU)}{\partial x} = 0 \\ \dfrac{\partial U}{\partial t} + U\dfrac{\partial U}{\partial x} + \dfrac{1}{\rho}\dfrac{\partial p}{\partial x} + \dfrac{2}{\rho}(\zeta + 2)\kappa\pi U = 0 \end{cases} \tag{17}$$

Finalised with eqn (14). In this chapter, we want to derive the characteristic equations of the model. Characteristic equations give insight into the behaviour of the model and will become useful during the implementation of the model.

4.1 Conservative form

Before we can derive the characteristic equations it is wise to write the derived system into a conservative form. The conservative form has the following form

$$\frac{\partial \mathbf{W}}{\partial t} + \frac{\partial F(\mathbf{W})}{\partial x} = S(\mathbf{W}) \tag{18}$$

We let $\mathbf{W}$ be the conserved quantity, $F(\mathbf{W})$ is the flux function, and $S(\mathbf{W})$ is the source function. So following eqn (17)

$$\begin{aligned} \mathbf{W} &= \begin{bmatrix} A \\ U \end{bmatrix} \\ F(\mathbf{W}) &= \begin{bmatrix} AU \\ \dfrac{1}{2}U^2 + \dfrac{p}{\rho} \end{bmatrix} \\ S(\mathbf{W}) &= \begin{bmatrix} 0 \\ -\dfrac{2}{\rho}(\zeta + 2)\kappa\pi U \end{bmatrix} \end{aligned} \tag{19}$$

Eqn (18) will be the starting point of the numerical methods described later.

4.2 Characteristic equations

As we have written the system in its conservative form we are now in the position to derive the characteristic equations. In order the derive the characteristic equations we should rewrite system 18 once more into the following form

$$\frac{\partial \mathbf{W}}{\partial t} + \mathbf{H}\frac{\partial \mathbf{W}}{\partial x} = K(\mathbf{W}) \tag{20}$$

For this, consider eqn (14) and assume $\beta = \beta(x)$, $p_{ext} = 0$ and $A_0 = A_0(x)$. First, we apply the chain rule

$$\frac{\partial p}{\partial x} = \frac{\partial p}{\partial A}\frac{\partial A}{\partial x} + \frac{\partial p}{\partial A_0}\frac{\partial A_0}{\partial x} + \frac{\partial p}{\partial \beta}\frac{\partial \beta}{\partial x} = \frac{\beta}{2\sqrt{A}}\frac{\partial A}{\partial x} - \frac{\beta}{2\sqrt{A_0}}\frac{\partial A_0}{\partial x} + (\sqrt{A} - \sqrt{A_0})\frac{\partial \beta}{\partial x} \tag{21}$$

Substituting this into eqn (17) and applying the chain rule on $\frac{\partial(AU)}{\partial x}$ we rewrite 20 into

$$\begin{bmatrix} A \\ U \end{bmatrix}_t + \begin{bmatrix} U & A \\ \dfrac{\beta}{2\rho\sqrt{A}} & U \end{bmatrix} \begin{bmatrix} A \\ U \end{bmatrix}_x = \begin{bmatrix} 0 \\ -\dfrac{2}{\rho}(\zeta+2)\kappa\pi U - \dfrac{1}{\rho}(\sqrt{A}-\sqrt{A_0})\dfrac{\partial\beta}{\partial x} + \dfrac{\beta}{2\rho\sqrt{A_0}}\dfrac{\partial A_0}{\partial x} \end{bmatrix} \tag{22}$$

The matrix $\mathbf{H} = \dfrac{\partial F(\mathbf{W})}{\partial W}$ is known as the flux Jacobian matrix and has eigenvalues equal to $\lambda_{1,2} = U \pm \sqrt{\dfrac{\sqrt{A}\beta}{2\rho}} = U \pm c$ when we define $c = \sqrt{\dfrac{\beta}{2\rho}} A^{\frac{1}{4}}$. c can be seen as the wave speed in the case the fluid is at rest. When the fluid moves with some velocity U, the waves are traveling with a velocity equal to $\lambda_{1,2}$. Note c can only be defined if $A > 0$, $\beta > 0$ and $\rho > 0$. In physical cases like the human body, this is the case. In [1] it has been shown that in the circulatory system $U < c$ hence we have that $\lambda_1 = U + c > 0$ and $\lambda_2 = U - c < 0$. We can now make two observations. Firstly, we note that the eigenvalues of system 17 are distinct and real. This means that the system is hyperbolic and subcritical [14]. Furthermore, we can now understand the system as two waves propagating through the fluid. One moves forwards with speed $(U + c)$ and one moves backward with speed $(U - c)$.

As we have now found the eigenvalues of this hyperbolic system we can use this to rewrite eqn (20). First note the matrix of left eigenvalues, $\mathbf{L}$, of $\mathbf{H}$ can be written as

$$\mathbf{L} = \begin{bmatrix} \dfrac{c}{A} & 1 \\ -\dfrac{c}{A} & 1 \end{bmatrix} \tag{23}$$

where

$$\mathbf{LH} = \mathbf{\Lambda L}$$
$$\mathbf{\Lambda} = \begin{bmatrix} U+c & 0 \\ 0 & U-c \end{bmatrix}$$

Note that we can write $\mathbf{H} = \mathbf{L^{-1}\Lambda L}$ so

$$\mathbf{L}\frac{\partial \mathbf{W}}{\partial t} + \mathbf{\Lambda L}\frac{\partial \mathbf{W}}{\partial x} = \mathbf{L}K(\mathbf{W}) \tag{24}$$

We are now in the position to introduce the characteristic variables $\mathbf{S} = \begin{bmatrix} s_1 \\ s_2 \end{bmatrix}$. We use that $\frac{\partial \mathbf{S}}{\partial \mathbf{W}} = \mathbf{L}$ as this simplifies the analysis a lot. This transforms eqn (24) into

$$\frac{\partial \mathbf{S}}{\partial \mathbf{W}}\frac{\partial \mathbf{W}}{\partial t} + \mathbf{\Lambda}\frac{\partial \mathbf{S}}{\partial \mathbf{W}}\frac{\partial \mathbf{W}}{\partial x} = \frac{\partial \mathbf{S}}{\partial \mathbf{W}}K(\mathbf{W}) \tag{25}$$

To simplify this equation we need information about the two different characteristic variables s_1 and s_2. Luckily these can be computed relatively easily using $\frac{\partial \mathbf{S}}{\partial \mathbf{W}} = \mathbf{L}$

$$\begin{bmatrix} \dfrac{\partial s_1}{\partial A} & \dfrac{\partial s_1}{\partial u} \\ \dfrac{\partial s_2}{\partial A} & \dfrac{\partial s_1}{\partial A} \end{bmatrix} = \begin{bmatrix} \dfrac{c}{A} & 1 \\ -\dfrac{c}{A} & 1 \end{bmatrix} \tag{26}$$

Solving these differential equations yield

$$s_1 = U + 4c = U + 4A^{\frac{1}{4}}\sqrt{\frac{\beta}{2\rho}}, \quad s_2 = U - 4c = U - 4A^{\frac{1}{4}}\sqrt{\frac{\beta}{2\rho}} \tag{27}$$

Since $\beta > 0$, we may write the variables (A, U) into the variables (s_1, s_2)

$$A = \left(\frac{s_1 - s_2}{4}\right)^4 \left(\frac{\rho}{2\beta}\right)^2, \quad U = \frac{s_1 + s_2}{2} \tag{28}$$

Since we now have computed the characteristic variables we can go back to simplifying eqn (25) by using the chain rule.

$$\frac{\partial \mathbf{S}}{\partial t} = \frac{\partial \mathbf{S}}{\partial \mathbf{W}} \frac{\partial \mathbf{W}}{\partial t}, \quad \frac{\partial \mathbf{S}}{\partial x} = \frac{\partial \mathbf{S}}{\partial \mathbf{W}} \frac{\partial \mathbf{W}}{\partial x} + \frac{\partial \mathbf{S}}{\partial \beta} \frac{\partial \beta}{\partial x} \tag{29}$$

We can use this identity to write

$$\frac{\partial \mathbf{S}}{\partial t} + \mathbf{\Lambda} \frac{\partial \mathbf{S}}{\partial x} = \mathbf{L} K(\mathbf{S}) + \mathbf{\Lambda} \frac{\partial \mathbf{S}}{\partial \beta} \frac{\partial \beta}{\partial x} \tag{30}$$

In the case that the friction is neglectable, $A_0(x) = A(x)$ and $\beta(x) = \beta$ we gain the final equations

$$\begin{aligned} \frac{\partial s_1}{\partial t} + \lambda_1 \frac{\partial s_1}{\partial x} &= 0 \\ \frac{\partial s_2}{\partial t} + \lambda_2 \frac{\partial s_2}{\partial x} &= 0 \end{aligned} \tag{31}$$

Looking at eqn (31) one can recognize a standard transport equation in it. This means that we can indeed understand the solution of the model as two waves traveling in opposite directions with velocity $\lambda_{1,2}$. Note that the two transport equations are coupled as $\lambda_1 = U + c = \frac{s_1 + s_2}{2} + \sqrt{\frac{\beta}{2\rho}} \frac{s_1 - s_2}{4} \sqrt{\frac{\rho}{2\beta}} = \frac{5s_1 + 3s_2}{8}$ and similarly $\lambda_2 = \frac{5s_2 + 3s_1}{8}$. The characteristic equations we have derived will be of great importance once we introduce the numerical parts.

5 Linear system

We have derived the system of PDEs to describe the blood transport through the arterial system (17). This system is coupled and therefore difficult to solve analytically. Therefore we use numerical methods to solve the system.

As we have seen before, eqn (17) is nonlinear but also strictly hyperbolic. Hyperbolic PDEs arise in a wide range of transport and wave propagation problems. In these problems, and ours in particular, the conservation of momentum and mass plays an important role. For this reason, we will use Finite Volume Method (FVM) as our integration method. As FVM has the property that mass and momentum are conserved.

5.1 Derivation of Finite Volume scheme

For the derivation of the Finite Volume Scheme, we follow the steps taken by LeVeque [6]. Like our system, FVM is derived using conservation laws. This is a great advantage. Note that our problem is defined in one dimension. In the spatial dimension, the FVM is based on subdividing the domain into subintervals, known as the *Finite Volumes*. The main idea is to keep track of the conserved variable in each of these subintervals. This quantity will be updated at each time step using the net flux in and out of the subintervals. This is schematically depicted in figure 2.

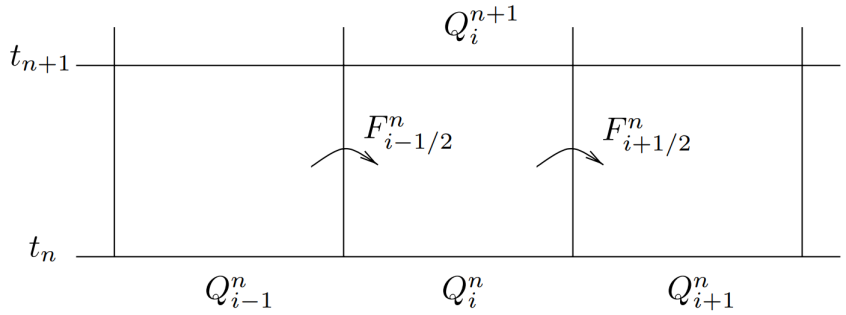

Figure 2: Schematic model of the Finite Volume Method from LeVeque [6]. The vertical axis depicts one timestep and horizontally you can see three subintervals shown. F symbolizes the flux moving from one cell to another. Q symbolizes the value of the conserved variable and is a 2-dimensional vector.

We denote the subinterval as $C_i = [x_{i-\frac{1}{2}}, x_{i+\frac{1}{2}}]$ with length Δx. In each subinterval, we will define the cell average of the conserved quantity $q(x, t^n)$ as $Q_i^n \equiv \frac{1}{\Delta x}\int_{C_i} q(x, t^n)dx$. In our system, Q is a 2-dimensional vector. The next step will be to look at the flux in each subinterval, $f(x, t^n)$. Using the same analogy as for deriving eqn (5).

$$\frac{d}{dt}\int_{C_i} q(x,t)dx = f(q(x_{i-\frac{1}{2}},t)) - f(q(x_{i+\frac{1}{2}},t)) \tag{32}$$

If we integrate both sides over one time step t_{n+1} to t_n and devide by Δx we arive at

$$\frac{1}{\Delta x}\int_{C_i} q(x,t_{n+1})dx - \frac{1}{\Delta x}\int_{C_i} q(x,t_n)dx = \frac{1}{\Delta x}\int_{t_n}^{t_{n+1}} f(q(x_{i-\frac{1}{2}},t))dt - \frac{1}{\Delta x}\int_{t_n}^{t_{n+1}} f(q(x_{i+\frac{1}{2}},t))dt \tag{33}$$

Now if we define the flux in each subinterval as $F^n_{i+\frac{1}{2}} = \frac{1}{\Delta t}\int_{t_n}^{t_{n+1}} f(q(x_{i+\frac{1}{2}},t))dt$. We arrive at the general numerical schematic for FVM:

$$Q_i^{n+1} = Q_i^n - \frac{\Delta t}{\Delta x}(F^n_{i+\frac{1}{2}} - F^n_{i-\frac{1}{2}}) \tag{34}$$

The problem with this scheme is that we cannot evaluate $F^n_{i\pm\frac{1}{2}}$ explicitly as we have no prior information about $q(x_{i\pm\frac{1}{2}},t)$. To tackle this problem in the linear case we remember that the information will propagate as waves over the characteristics. Using this knowledge could create better expressions for the numerical flux. This idea has given rise to first-order Godunuv's Method [15]. Please see [6] for the derivation of the flux function which we will take here without justification.

$$Q_i^{n+1} = Q_i^n - \frac{\Delta t}{\Delta x}(\mathbf{A}^+\Delta Q^n_{i-\frac{1}{2}} + \mathbf{A}^-\Delta Q^n_{i+\frac{1}{2}}) \tag{35}$$

Here $\mathbf{A}^+\Delta Q^n_{i-\frac{1}{2}}$ represents the flux of the right moving wave at the border between x_i and x_{i-1}. Similarly $\mathbf{A}^-\Delta Q^n_{i+\frac{1}{2}}$ represents the flux of the left moving wave between x_i and x_{i+1}. $\mathbf{A}$ is here the hyperbolic matrix which can be diagonalized as $\mathbf{A} = \mathbf{R\Lambda R^{-1}}$. $\mathbf{\Lambda}$ is the matrix with the eigenvalues and $\mathbf{R}$ the matrix of right eigenvectors. If we create $\mathbf{\Lambda}^+$ with only positive eigenvalues and $\mathbf{\Lambda}^-$ with only negative eigenvalues we can derive at

$$\mathbf{A}^+\Delta Q^n_{i-\frac{1}{2}} = \mathbf{R\Lambda}^+\mathbf{R^{-1}}(Q_i^n - Q^n_{i-1}), \quad \mathbf{A}^-\Delta Q^n_{i+\frac{1}{2}} = \mathbf{R\Lambda}^-\mathbf{R^{-1}}(Q^n_{i+1} - Q_i^n) \tag{36}$$

We can now understand eqn (35). The only way Q can change is due to waves propagating to the left, which would be coming from the right boundary, or waves propagating to the right, which would be coming from the left boundary. Their sum would then account for the total change in Q. This is exactly what the numerical scheme tells us.

5.2 Stability

For our numerical method to be stable and convergent there is a necessary condition which must be satisfied. As we have seen, information in our system is propagating as waves over the characteristic equations. Assume that these waves are traveling with velocity λ. In this way, the solution is translated over a distance $\Delta t|\lambda|$ in each time step. Since the flux function at point $x_{i-\frac{1}{2}}$ is dependent on Q^n_{i-1} and Q^n_i, information should not be traveling more than a grid cell at each time step. This principle is a consequence of the CFL condition (Courant, Friedrichs, and Lewy). It hence gives some conditions on the time and spatial discretization. It must be satisfied that:

$$\text{CFL} \equiv \frac{|\lambda|\Delta t}{\Delta x} \leq 1 \tag{37}$$

The value of this quotient is called the Courant Number and it tells us that the solution can only be traveling one subinterval each time step.

5.3 Linear test case

To get a better feeling for the FVM, we start exploring a linear test case. Consider the following problem:

$$\frac{\partial \mathbf{q}}{\partial t} + \mathbf{A}\frac{\partial \mathbf{q}}{\partial x} = \begin{bmatrix} q_1 \\ q_2 \end{bmatrix}_t + \begin{bmatrix} 2 & 3 \\ 3 & 2 \end{bmatrix}\begin{bmatrix} q_1 \\ q_2 \end{bmatrix}_x = \begin{bmatrix} 0 \\ 0 \end{bmatrix} \tag{38}$$

To be able to implement the numerical scheme in eqn (35) we need to diagonalize matrix $\mathbf{A}$. Computing the eigenvalues gives us $\lambda_1 = 5$ and $\lambda_2 = -1$. Note that these eigenvalues are distinct and real, so the system is indeed hyperbolic as desired. After computing the eigenvectors we can write:

$$\mathbf{A} = \mathbf{R}\mathbf{\Lambda}\mathbf{R^{-1}} = \frac{1}{\sqrt{2}}\begin{bmatrix}1 & -1\\ 1 & 1\end{bmatrix}\begin{bmatrix}5 & 0\\ 0 & -1\end{bmatrix}\frac{1}{\sqrt{2}}\begin{bmatrix}1 & 1\\ -1 & 1\end{bmatrix} \tag{39}$$

Knowing this we can follow eqn (36) and define

$$\mathbf{\Lambda}^+ = \begin{bmatrix}5 & 0\\ 0 & 0\end{bmatrix} \quad \mathbf{\Lambda}^- = \begin{bmatrix}0 & 0\\ 0 & -1\end{bmatrix} \tag{40}$$

We are now almost in the position to apply eqn (35).

5.3.1 Characteristic variables

Before we analyse the FVM we again take a look at the characteristic variables as they can tell us much about the behavior of the solution. So, let us compute the characteristic variables for our linear test case similarly as done in chapter 4.

$$\begin{aligned}&\mathbf{q}_t + \mathbf{R}\mathbf{\Lambda}\mathbf{R^{-1}}\mathbf{q_x} = 0\\ &\mathbf{R^{-1}}\mathbf{q_t} + \mathbf{\Lambda}\mathbf{R^{-1}}\mathbf{q_x} = 0\end{aligned} \tag{41}$$

When we now define the characteristic variables s_1 and s_2 as $\mathbf{S} = [s_1 s_2]^T = \mathbf{R^{-1}}\mathbf{q}$. We arrive at the characteristic equations.

$$\begin{aligned}&\frac{\partial s_1}{\partial t} + \lambda_1\frac{\partial s_1}{\partial x} = 0\\ &\frac{\partial s_2}{\partial t} + \lambda_2\frac{\partial s_2}{\partial x} = 0\end{aligned} \tag{42}$$

We again see that the problem decomposes into two scalar transfer equations. Since $\lambda_1 > 0$ and $\lambda_2 < 0$ we note that we again have a right traveling wave with velocity λ_1 and a left traveling wave with velocity λ_2.

5.4 Boundary conditions

So far we have seen a numerical scheme to compute to cell average Q_i^n. However, in any problem, we only deal with a finite grid which gives rise to boundary values. Dealing with boundary conditions can be difficult but the characteristic variables turn out to be useful. We remember that the solution is a combination of the forward and backward traveling waves. At a given boundary we should thus only define the incoming wave. This means that at the left boundary, characteristic variable s_1 with velocity λ_1 should be prescribed. On the other side, characteristic variable s_2 with velocity λ_2 should be prescribed. However, sometimes we want to describe the boundary conditions in terms of our original variables, which are q_1 and q_2 in the test case. Gauily and Epstein [16] have shown that to determine which of the original variable can be used to describe the boundaries one needs to have a non-zero Jacobian. So it must satisfy that

$$\mathbf{J} = \frac{\partial \mathbf{q}}{\partial \mathbf{S}} \neq \mathbf{0} \tag{43}$$

We can use a variable to prescribe a characteristic if the corresponding element of J_{s_i} is non-zero. Looking at the right boundary which is prescribed by s_2 we compute

$$\frac{\partial \mathbf{q}}{\partial s_2} = \begin{bmatrix} -\frac{1}{\sqrt{2}} \\ \frac{1}{\sqrt{2}} \end{bmatrix} \tag{44}$$

Here we have used that $\mathbf{S} = \mathbf{R^{-1}q}$. Since neither $\frac{\partial q_1}{\partial s_2}$ nor $\frac{\partial q_2}{\partial s_2}$ equals zero, the right boundary can be described by either q_1 or q_2. A similar analysis on the left boundary shows that also the left boundary can be described by both q_1 as q_2.

5.5 Analysis of the linear test case

We have now developed all the tools to analyse the Finite Volume Method in a linear case. With the addition of the boundary and initial conditions, the problem is as follows:

$$\begin{bmatrix} q_1 \\ q_2 \end{bmatrix}_t + \begin{bmatrix} 2 & 3 \\ 3 & 2 \end{bmatrix} \begin{bmatrix} q_1 \\ q_2 \end{bmatrix}_x = \begin{bmatrix} 0 \\ 0 \end{bmatrix} \tag{45}$$

$$\text{IC: } \begin{bmatrix} 1 + e^{-50(x-\frac{1}{2})^2} \\ 1 \end{bmatrix} \quad \text{BC1: } q_1(0,t) = 1 + \frac{1}{20}\sin(2\pi t) \quad \text{BC2: } s_2(1,t) = 0$$

Defined on the interval $0 < x < 1$ and $t > 0$.

We have chosen as an initial condition an exponentially decaying function. This creates a clear peak in the middle of the interval which can then be easily analysed. The sinus function as a boundary was chosen since these waves are very recognizable. This enables us to see the influence of the boundary more clearly. However, the amplitude of the sinus is chosen very small in comparison to the amplitude of the exponential function such that it does not overpower this initial peak. The right boundary $s_2(0,t) = 0$ simply means there is no left-moving wave at this boundary. We see that this formulation of the boundaries is valid as $\frac{\partial q_1}{\partial s_1} \neq 0$.

5.5.1 Implementation of the boundary conditions

For the numerical computation, note that the interior can easily be computed when combining eqn (35) with eqn (36). However, the boundaries should be looked at with extra care. For the handling of these boundaries, we follow LeVeque [6]. To this end, we extend our computation domain by adding additional volumes on both sides of the domain. These extra cells, Q^n_{N+1} and Q^n_0 are referred to as *Ghost cells*. These ghost cells will be used for the numerical scheme at the boundary. Let us first look at the right boundary.

The right boundary condition implies that there are no left-traveling waves here. This implies that the ghost cell Q^n_{N+1} has the same value as the last cell Q^n_N.

$$\mathbf{A}^-\Delta Q^n_{i+\frac{1}{2}} = \mathbf{R\Lambda^+R^{-1}}(Q^n_{N+1} - Q^n_N) = \mathbf{R\Lambda^+R^{-1}}(Q^n_N - Q^n_N) = 0 \tag{46}$$

So at the right boundary, this numerical scheme becomes

$$Q^{n+1}_N = Q^n_N - \frac{\Delta t}{\Delta x}\mathbf{A}^+\Delta Q^n_{N-\frac{1}{2}} \tag{47}$$

For the left boundary, we have a condition on the solution q_1. We again define a ghost cell but this time on the left end, Q^n_0. Note that we have previously found that $\mathbf{S} = \mathbf{R^{-1}q}$ and so $\begin{bmatrix} q_1 \\ q_2 \end{bmatrix} = \begin{bmatrix} \frac{1}{\sqrt{2}}(s_1 - s_2) \\ \frac{1}{\sqrt{2}}(s_1 + s_2) \end{bmatrix}$

This also means $q_1(0,t) = \frac{1}{\sqrt{2}}(s_1 - s_2)$. Remember that s_1 is the right traveling characteristic and s_2 is the left traveling characteristic. So s_2 can just be computed inside the computational domain. It follows that $s_1(0,t) = s_2(0,t) + \sqrt{2}q_1(0,t)$. We can now define the value of the ghost cell Q_0^n:

$$Q_0^n = \mathbf{RS} = \begin{bmatrix} \frac{1}{\sqrt{2}}(s_1(0,t_n) - s_2(0,t_n)) \\ \frac{1}{\sqrt{2}}(s_1(0,t_n) + s_2(0,t_n)) \end{bmatrix} = \begin{bmatrix} q_1(0,t) \\ \sqrt{2}s_2(0,t_n) + q_1(0,t) \end{bmatrix} \tag{48}$$

So the numerical flux function becomes

$$\mathbf{A}^+ \Delta Q^n_{i-\frac{1}{2}} = \mathbf{R}\mathbf{\Lambda}^+\mathbf{R}^{-\mathbf{1}}(Q_1^n - Q_0^n) \tag{49}$$

with Q_0^n as defined in eqn (48).

5.5.2 Results

We solve the linear test case from eqn (45) in the programming language Python [17]. The time step is taken at $\Delta t = 0.001$ and the space step at $\Delta x = 0.01$. This gives a Courant Number of 0.5. Note that this test case is not based on any physical phenomena but a purely mathematical one. In figure 3 the results are shown of q_1 together with the analytical solution.

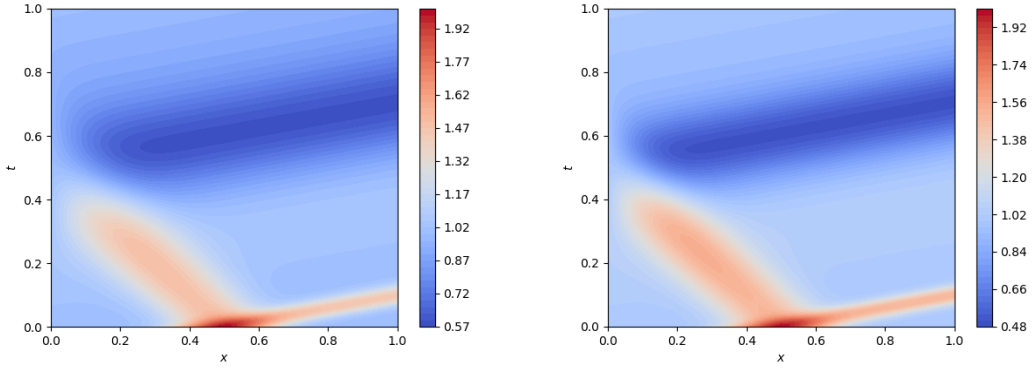

(a) Numerical solution of q_1 of the test case

(b) Analytical solution of q_1 of the linear test case

Figure 3: The plot shows the comparison between the numerical solution and analytical solution of the variable q_1 of the linear test case.

The analytical solution was computed following Roosendaal [8]. Let us first look at the overall behaviour of the solution. When looking at figure 3 we first note that at $t = 0$ we indeed have a peak around the $x = 0.5$. From there we see the peak decomposing in two waves traveling in opposite directions. The right propagating one reaches the wall around $t = 0.1$. This implies that it was moving with a velocity of $v = \frac{\Delta x}{\Delta t} = \frac{0.5}{0.1} = 5$. This is exactly what we expected as $\lambda_1 = 5$. Similarly, we see that the left propagating wave reaches the left wall at $t = 0.5$. So the velocity of the left propagating wave is $v = \frac{\Delta x}{\Delta t} = \frac{-0.5}{0.5} = -1$. This is also what we would expect as $\lambda_2 = -1$. This shows us that indeed the solution can be seen as two waves propagating in opposite directions. Let us now look at the influence of the boundary conditions. We would expect no effect on the solution at the right boundary. This is indeed what we see in figure 3. On the other hand, the left boundary does affect the solution. We see that the left boundary resembles a sine wave. The wave 'flips' at the boundary which is as expected. Let us now

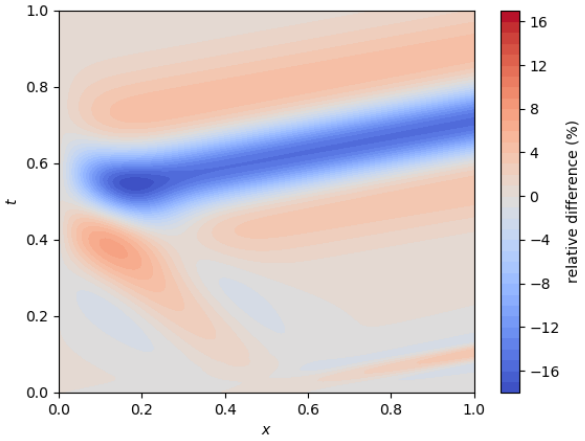

Figure 4: This figure shows the relative difference between the analytical and numerical solution of the test case.

compare the results with the analytical solution. We first note that the numerical and analytical computed solutions are very similar. This gives us confidence about using the first-order Godunuv's Method. However, there is an important difference notable between the solutions. Our numerically computed solutions seem to be diluted. This can be seen in the intensity graphs of the solutions. In figure 4 the relative difference between the analytical and numerical solution of eqn. (45) is seen. Note that the diffusion is mostly present at the reflected wave. This is a known effect of first-order Godunuv but the numerical diffusion can be greatly reduced by using a finer grid.

6 Nonlinear system

Up till now, we have investigated the Finite Volume Method for a linear case. However, as we have derived in Chapter 2, the system of equations 17 is nonlinear. This makes that we cannot use the numerical difference scheme 35 which we derived before. To this end, we look at the inflow and outflow at the boundaries of the cell.

6.1 Riemann problem

We will consider the Riemann problem. This is a specific initial value problem composed of a conservation equation together with a piece-wise constant initial data with a *single* discontinuity. For simplicity, we first consider the case when the frictional terms can be neglected. Hence system 17 can be written in a conservative form as

$$\frac{\partial \mathbf{W}}{\partial t} + \frac{\partial F(\mathbf{W})}{\partial x} = \mathbf{0} \tag{50}$$

Again we used that

$$\begin{aligned} \mathbf{W} &= \begin{bmatrix} A \\ U \end{bmatrix} \\ F(\mathbf{W}) &= \begin{bmatrix} AU \\ \frac{1}{2}U^2 + \frac{p}{\rho} \end{bmatrix} \end{aligned} \tag{51}$$

Like in our previous derivation of the numerical scheme, we consider subintervals $C_i = [x_{i-\frac{1}{2}}, x_{i+\frac{1}{2}}]$ with length Δx. We consider the average value of the conserved variable $\mathbf{W}$ at interval C_i and time t^n as $\mathbf{W}_i^n = \frac{1}{\Delta x}\int_{C_i} \mathbf{W}(x, t^n)dx$. We will now investigate what happens at the boundary between the i-th cell and the $i-1$-the cell. Note that here we have piece-wise constant data:

$$\mathbf{W}(x, t^n) = \begin{cases} \mathbf{W}_i^n & x < x_{i-\frac{1}{2}} \\ \mathbf{W}_{i-1}^n & x > x_{i-\frac{1}{2}} \end{cases} \tag{52}$$

Here the discontinuity appears at the border of the two cells, at $x_{i-\frac{1}{2}}$, as we will prove in a moment. So we have indeed a Riemann problem. Now the aim is to use the solution of this Riemann problem to find the solution one time-step further so $\mathbf{W}_i^{n+1}$ and $\mathbf{W}_{i-1}^{n+1}$. Unfortunately, we cannot simply use eqn (35) because the flux function $F(\mathbf{W}, x)$ is nonlinear. To solve this, we follow Bale and LeVeque [18] to use a method based on flux difference decomposition.

We first use some linearizations to simplify the problem. As done in [18] we use *cell-centered flux functions*. For this approach, we assume that the flux function is constant inside each subinterval so $F(\mathbf{W}, x_i) = F_i(\mathbf{W})$. So the *generalized* Riemann problem, which by the CFL-condition is only valid for $x \in [x_{i-\frac{2}{3}}, x_{i+\frac{1}{2}}]$, becomes:

$$\begin{aligned} \frac{\partial \mathbf{W}}{\partial t} + \frac{\partial F_{i-1}(\mathbf{W})}{\partial x} &= \mathbf{0} \quad x < x_{i-\frac{1}{2}} \\ \frac{\partial \mathbf{W}}{\partial t} + \frac{\partial F_i(\mathbf{W})}{\partial x} &= \mathbf{0} \quad x > x_{i-\frac{1}{2}} \end{aligned} \tag{53}$$

We will now take a closer look at this Riemann problem to prove that we indeed have a discontinuity. Figure 5 shows the domain of the Rieman problem.

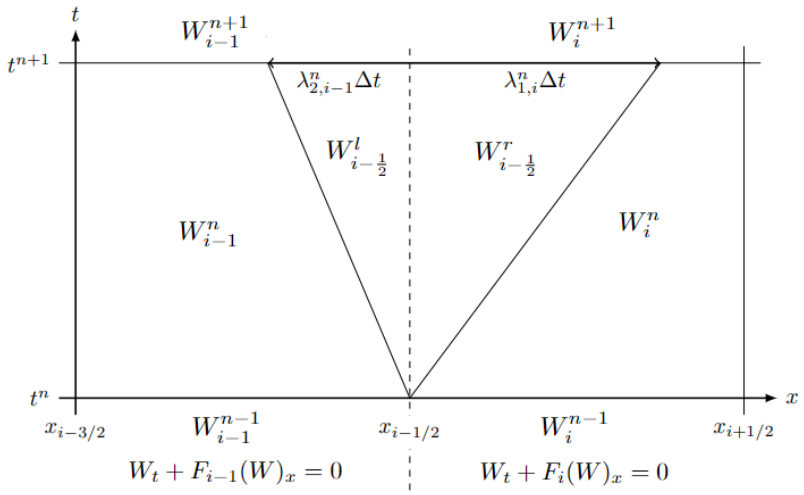

Figure 5: Schematic of the domain of the Riemann problem [8]. The vertical axis shows a single time step and the horizontal axis shows two intervals C_i and C_{i-1}. The dashed line depicts the border. In each enclosed area, the name of the solution is written. So W_{i-1}^n means the solution at t^n and C_i.

As we have seen in chapter 4, we expect our solution to be decomposed into waves. For eqn (53) we expect information to travel with velocity $\lambda_{1,i-\frac{1}{2}}^n$ and $\lambda_{2,i-\frac{1}{2}}^n$. In one time-step Δt only a distance $\lambda_{1/2,i-1}^n \Delta t$ can be traveled. This is depicted in figure 5. Here the vertical axis shows a single time step t^n to t^{n+1}. The horizontal axis shows two subintervals C_i and C_{i-1} with the dashed line on their border. The diagonal line is the border of the parts which *have* received information about the solution and parts which *have not*. So at each time, the x-coordinate of this diagonal line tells us how far information coming from $x_{i-\frac{1}{2}}$ has traveled. Thus the value of $\mathbf{W}$ in each enclosed area must be constant. In the figure, $\mathbf{W}_{i-\frac{1}{2}}^l$ and $\mathbf{W}_{i-\frac{1}{2}}^r$ denotes the value of $\mathbf{W}$ left and right of the cell-border respectively. Because we expect the flux the be conserved we have $F_{i-1}(\mathbf{W}_{i-\frac{1}{2}}^l) = F_i(\mathbf{W}_{i-\frac{1}{2}}^r)$. But in general $F_{i-1}(\mathbf{W}) \neq F_i(\mathbf{W})$. From this it must follow that $\mathbf{W}_{i-\frac{1}{2}}^l \neq \mathbf{W}_{i-\frac{1}{2}}^r$. So we have proven that there is indeed a discontinuity at each cell interface.

The fact that we have a discontinuity makes this problem a lot harder. We continue our search for a numerical scheme to solve the system from 17. We follow analogously as in chapter 4. For this, we apply the chain rule to eqn (53).

$$\begin{aligned} \frac{\partial \mathbf{W}}{\partial t} + \frac{\partial F_{i-1}(\mathbf{W})}{\partial \mathbf{W}} \frac{\partial \mathbf{W}}{\partial x} = 0 \quad x < x_{i-\frac{1}{2}} \\ \frac{\partial \mathbf{W}}{\partial t} + \frac{\partial F_i(\mathbf{W})}{\partial \mathbf{W}} \frac{\partial \mathbf{W}}{\partial x} = 0 \quad x < x_{i-\frac{1}{2}} \end{aligned} \tag{54}$$

Note that the source terms from eqn (20) drop out since β and A_0 are assumed to be constant. Here we again find the flux Jacobian matrix $H(\mathbf{W}, x_i) = \frac{\partial F(\mathbf{W})}{\partial \mathbf{W}}$ which was already found to be

$$H(\mathbf{W}) = \begin{bmatrix} U & A \\ \dfrac{\beta}{2\rho\sqrt{A}} & U \end{bmatrix} \tag{55}$$

We assume that the flux Jacobian matrix is constant in each cell. So we write $H(\mathbf{W}, x_i) = H_i(\mathbf{W}) = \mathbf{H}_i^n$ in each cell C_i and time t^n. We have now reached a 2×2 linear system of PDEs. As we have seen in the

test case, such a system consists of two characteristics with constant eigenvectors and -values. So this is now the case as well. Since the system is subcritical, one of the characteristic variables is traveling to the right and one is traveling to the left.

Unlike in the linear case, we should carefully consider what happens at the discontinuity $x_{i-\frac{1}{2}}$. At any time t^n we have piece-wise constant initial data namely, $\mathbf{W}_i^n$ and $\mathbf{W}_{i-1}^n$. As a result, the characteristic variables are also piece-wise constant. We then expect the discontinuity at $x_{i-\frac{1}{2}}$ to travel left with velocity $\lambda_{2,i-1}^n$ into cell C_{i-1} and with velocity $\lambda_{1,i-1}^n$ into cell C_i. We thus find that the solution of $\mathbf{W}$ at time t^{n+1} is consisting of 4 values, $\mathbf{W}_i^n, \mathbf{W}_{i-1}^n, \mathbf{W}_{i-\frac{1}{2}}^l$ and $\mathbf{W}_{i-\frac{1}{2}}^r$. Moreover, we see that in each cell there are two more discontinuities. These discontinuities are the waves that determine the solution.

Remember that the eigenvectors and eigenvalues of $\mathbf{H}$ are given by:

$$\begin{aligned} \lambda_1 = U + c \quad \mathbf{r}_1 = \begin{bmatrix} \frac{A}{2c} \\ \frac{1}{2} \end{bmatrix} \\ \lambda_2 = U - c \quad \mathbf{r}_2 = \begin{bmatrix} -\frac{A}{2c} \\ \frac{1}{2} \end{bmatrix} \end{aligned} \tag{56}$$

With $\lambda_2 < 0 < \lambda_1$. We consider the cell C_i. For the first wave which travels right, we say

$$\lambda_{1,i-\frac{1}{2}}^n = \lambda_{1,i}^n \quad \mathbf{r}_{1,i-\frac{1}{2}}^n = \mathbf{r}_{1,i}^n \tag{57}$$

On the other hand, the second wave travels left. Therefore we can use the values of $\mathbf{W}_{i-1}^n$.

$$\lambda_{2,i-\frac{1}{2}}^n = \lambda_{2,i-1}^n \quad \mathbf{r}_{2,i-\frac{1}{2}}^n = \mathbf{r}_{2,i-1}^n \tag{58}$$

The classical Riemann problem for constant-coefficient systems is usually solved by using their eigenvectors. The standard approach is to decompose the jump in $\mathbf{W}$ as a linear combination of the eigenvectors. This linear combination then defines the waves $\mathcal{S}_{1/2,i-\frac{1}{2}}^n$:

$$\mathbf{W}_i - \mathbf{W}_{i-1} = \alpha_{1,i-\frac{1}{2}}\mathbf{r}_1 + \alpha_{2,i-\frac{1}{2}}\mathbf{r}_2 \equiv \mathcal{S}_{1,i-\frac{1}{2}} + \mathcal{S}_{2,i-\frac{1}{2}} \tag{59}$$

With

$$\alpha_{i-\frac{1}{2}} = \mathbf{L}_{i-\frac{1}{2}}(\mathbf{W}_i - \mathbf{W}_{i-1}) \tag{60}$$

where $\mathbf{L}$ is the matrix of left eigenvectors. However in our case we should also consider $\mathbf{W}_{i-\frac{1}{2}}^l$ and $\mathbf{W}_{i-\frac{1}{2}}^r$. Solving these directly is a difficult task therefore we will use the *flux wave decomposition* like in [18]. In this approach, instead of decomposing $(\mathbf{W}_i - \mathbf{W}_{i-1})$ we decompose $(F_i(\mathbf{W}) - F_{i-1}(\mathbf{W}))$ as a linear combination of eigenvectors. This linear combination defines the *flux waves* $\mathcal{Z}_{i-\frac{1}{2}}^n$. We get

$$F_i(\mathbf{W}) - F_{i-1}(\mathbf{W}) = \mathcal{Z}_{1,i-\frac{1}{2}}^n + \mathcal{Z}_{2,i-\frac{1}{2}}^n = \gamma_{1,i-\frac{1}{2}}^n \mathbf{r}_{1,i}^n + \gamma_{2,i-\frac{1}{2}}^n \mathbf{r}_{2,i-1}^n \tag{61}$$

We can see γ as the relative strength of the eigenvectors. Solving for γ yields

$$\begin{bmatrix} \gamma_{1,i-\frac{1}{2}} \\ \gamma_{2,i-\frac{1}{2}} \end{bmatrix} = \frac{2}{\frac{A_i^n}{c_i^n} + \frac{A_{i-1}^n}{c_{i-1}^n}} \begin{bmatrix} 1 & \frac{A_{i-1}^n}{c_{i-1}^n} \\ 1 & \frac{A_i^n}{c_i^n} \end{bmatrix} (F_i(\mathbf{W}) - F_{i-1}(\mathbf{W})) \tag{62}$$

We can now define the j-th flux waves as $\mathcal{Z}_{j,i-\frac{1}{2}} = \gamma^n_{j,i-\frac{1}{2}} r^n_{j,i-\frac{1}{2}}$. These waves are the net effect of all the waves propagating through the border of the cell. We can now substitute eqn (62) into eqn (34) to get the following numerical scheme

$$\mathbf{W}_i^{n+1} = \mathbf{W}_i^n - \frac{\Delta t}{\Delta x}(\mathbf{R}^+ \Delta \mathbf{W}^n_{i+\frac{1}{2}} + \mathbf{R}^- \Delta \mathbf{W}^n_{i-\frac{1}{2}}) = \mathbf{W}_i^n - \frac{\Delta t}{\Delta x}(\mathcal{Z}^n_{1,i-\frac{1}{2}} + \mathcal{Z}^n_{2,i-\frac{1}{2}}) \tag{63}$$

6.2 Boundary conditions

Similar to what we have done with the test case, we look at how we can prescribe the boundary conditions. Again we have two characteristic variables traveling with different velocities. We have that s_1 is traveling right with velocity $\lambda_1 > 0$ and s_2 is traveling left with velocity $\lambda_2 < 0$. This means that again s_1 should be prescribed at the left boundary and s_2 at the right boundary. We follow Gauily and Epstein [16] and check if eqn (43) holds. In this case, the original variables are A and U. First at the right boundary

$$\frac{\partial \mathbf{W}}{\partial s_1} = \begin{bmatrix} \left(\frac{s_1 - s_2}{4}\right)^3 \left(\frac{\rho}{2\beta}\right)^2 \\ \frac{1}{2} \end{bmatrix} \tag{64}$$

For the derivation, we have used eqn (28). Gauily and Epstein have shown that we can prescribe the boundary in terms of A and U if eqn (64) gives non-zero elements. We note that we can always describe the right boundary in terms of U as the element we find is $\frac{1}{2}$. Moreover, we see that we can describe the right boundary in terms of A if $s_1 \neq s_2$. But using eqn (27) we derive that

$$s_1 \neq s_2 \implies U + 4c \neq U - 4c \implies c \neq -c \implies c \neq 0 \tag{65}$$

And since we assume $c > 0$ we find that we can prescribe the right boundary by A or U. For the left boundary, we use 28 again to find

$$\frac{\partial \mathbf{W}}{\partial s_2} = \begin{bmatrix} -\left(\frac{s_1 - s_2}{4}\right)^3 \left(\frac{\rho}{2\beta}\right)^2 \\ \frac{1}{2} \end{bmatrix} \tag{66}$$

A similar analysis shows that also in the case of the left boundary, both A and U can be prescribed.

6.2.1 Forward prescribing

When specifying the incoming waves, this can be done via p, A, or U. Traditionally, this would force one of these variables to have a certain value at the boundary. However, in that way, knowledge is needed about the back traveling waves s_2 too. This would generally not be known as these waves also depend on for example the material property and the presence of bifurcations further in the domain. It is therefore often more convenient to prescribe the *forward* traveling wave (s_1) at the boundary and fix the *backward* traveling wave (s_2) at its initial value. This way of prescribing the boundaries is called *forward prescribing* [4]. It must be noted, however, that the *actual* value at the boundary will only be equal to the prescribed value of the boundary if no backward traveling waves arrive. When these waves do arrive, the actual value is not equal to the assigned value but consists of (prescribed) forward and backward terms. Nevertheless, this difference is very small and the non-reflective properties of forward prescribing are worth the difference.

6.3 Frictional forces

In deriving the numerical scheme of eqn (63) we have assumed the frictional forces to be neglectable. We now consider the case when these terms are non-neglectable. In eqn (19) we see that the frictional function is dependent on U. Therefore, we use first-order discretization to add the frictional forces to our method. This gives a second term in our method

$$\mathbf{W}_i^{n+1} = \mathbf{W}_i^n - \frac{\Delta t}{\Delta x}(\mathcal{Z}^n_{1,i-\frac{1}{2}} + \mathcal{Z}^n_{2,i-\frac{1}{2}}) + \Delta t S_i^n(\mathbf{W}) \tag{67}$$

where

$$S_i^n(\mathbf{W}) = \begin{bmatrix} 0 \\ -\frac{2}{\rho}(\zeta+2)\nu\pi U_i^n \end{bmatrix} \tag{68}$$

7 Test cases arteries

In the previous chapters, we have derived the knowledge needed to solve the system of eqn (17). Before we consider the entire human circulatory system we first consider different cases of single arteries. We investigate three different cases of arteries: a standard artery, a stented artery, and a tapered artery (this case can be found in the appendix). With these arteries, we investigate the flux differencing method and the effect of changing arterial properties on the pressure, velocity, and cross-sectional area of the different arteries.

7.1 Standard artery

We first consider a standard artery as this is the simplest case we could have. For this test case, we follow Sherwin et al. [1]. We assume a straight artery with a constant area and elasticity over the entire length. We prescribe the left boundary condition in terms of pressure following the section *forward prescribing*

$$p(0,t) = \begin{cases} 2000 \sin \frac{2\pi t}{T} & t < \frac{T}{2} \\ 0 & t > \frac{T}{2} \end{cases} \tag{69}$$

So we have defined an inflow pressure during half the period. Note that this way of defining the pressure ensures that the pressure is always positive. Moreover, a sin wave has a clear shape and can thus be easily investigated. The right boundary is a periodic boundary condition so

$$s_2(L,t) = s_2(0,t) \tag{70}$$

We can now implement these boundaries numerically.

7.1.1 Boundary conditions

First, we consider the left boundary. At $x = 0$ we can write eqn (14) as

$$p(0,t) = p_{ext} + \beta(\sqrt{A} - \sqrt{A_0}) \tag{71}$$

This influences the area at $x = 0$, hence with $p_{ext} = 0$

$$A = \left(\frac{p(0,t)}{\beta} + \sqrt{A_0} \right)^2 \tag{72}$$

We want to use the characteristic variables to define this boundary condition. So using eqn (28)

$$s_1 = s_2 + 4\sqrt{\frac{2\beta}{\rho}} A^{\frac{1}{4}} \implies s_1(0,t) = s_2(0,0) + 4\sqrt{\frac{2}{\rho}\left(p(0,t) + \beta\sqrt{A_0}\right)} \tag{73}$$

This equation can be implemented numerically. Moreover, note that the right boundary is described in terms of s_2 and can hence already be easily implemented.

7.1.2 Results standard artery

In the test case, we consider an artery of length $L = 15$ cm. Following Sherwin et al. [1] we take $\beta = 451352$, $\rho = 1$ and $A_0 = 0.5$. We have taken $\Delta x = 0.04$ cm. For choosing the size of the time step

we have to be careful. As explained in chapter 5 we should ensure that the CFL condition is satisfied so $\Delta t \leq \frac{\Delta x}{|\lambda|}$. But since λ is not constant over the domain we determine Δt at each time step such that

$$\Delta t^n = \frac{\Delta x}{|\lambda^n|_{max}} \tag{74}$$

Summarizing, we have

$$\text{IC: } \begin{bmatrix} A \\ U \end{bmatrix} = \begin{bmatrix} 0 \\ 0.5 \end{bmatrix} \quad \text{BC1: } p(0,t) = p_{ext} + \beta(\sqrt{A} - \sqrt{A_0}) \quad \text{BC2: } s_2(L,t) = s_2(0,t) \tag{75}$$

In figure 6 the results of the pressure wave are shown.

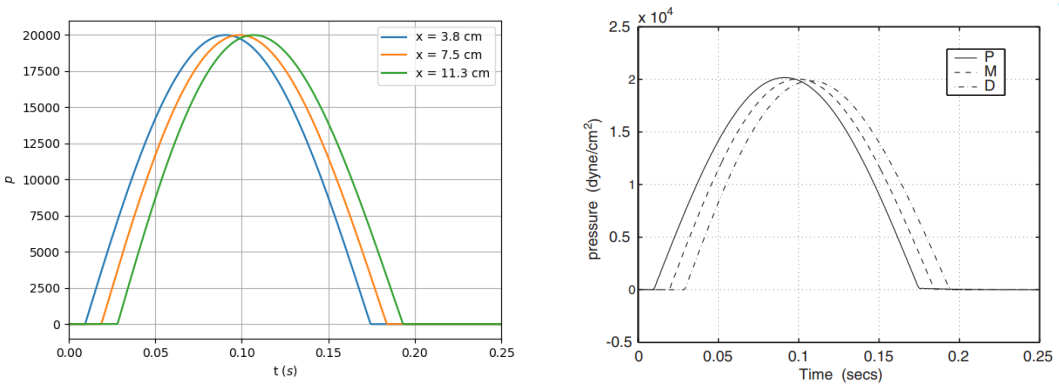

(a) Results of the standard artery in our model

(b) Results of the standard artery from Sherwin et al. [1]

Figure 6: Results of the test case of a standard artery. Subfigure (a) shows our results, and subfigure (b)is from Sherwin et al. In both cases, the pressure wave is plotted at $\frac{1}{4}$L, $\frac{1}{2}$L and $\frac{3}{4}$L.

We must first note that the approach [1] took is slightly different than we did. They used a discontinuous Galerkin scheme (for more information about the method please see [19]) while we used the flux differencing method. This said, we see that both methods are very comparable. We notice that the pressure wave, initiated at the boundary, is slowly propagating over the domain. We notice that the wave is undistorted, this is expected as the material properties are the same over the entire artery. Furthermore, we see that the results are not diffusive like the linear test case. The peak of the wave remains at the same level. This new flux difference splitting approach has thus eliminated the diffusive effects. So we can conclude that decomposing the flux function has this beneficial effect and works at least as well as the discontinuous Galerkin scheme in this case.

7.2 Stented artery

In the previous test case, we looked at how the pressure wave propagates in an artery with constant material properties. In the following test case, also done in [1], we consider the case when a small variation in the material properties is applied. We will look at a stented artery. Here, an expandable metal mesh coil is added in the middle of the artery. This is modeled as an increase in stiffness (β) at this part of the artery. Figure 7 shows this schematically.

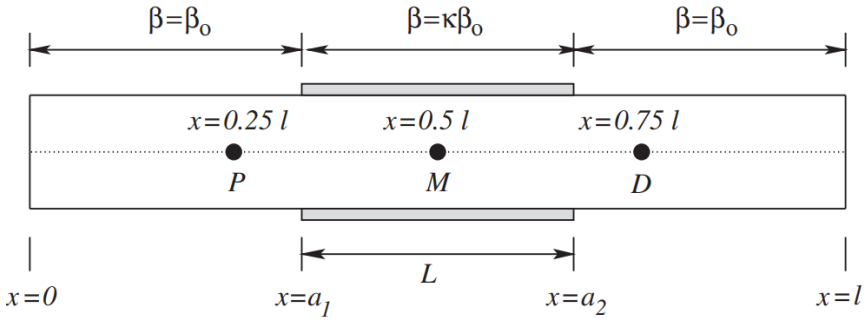

Figure 7: Schemetic representation of the stented artery from [1]

In this test case, we now let β be depending on x.

$$\beta(x) = \begin{cases} \beta_0 & 0 < x < a_1 \\ \beta_0 \kappa & a_1 < x < a_2 \\ \beta_0 & a_2 < x < L \end{cases} \tag{76}$$

We take $\beta_0 = 451352$ and $\kappa = 100$. Moreover, the stent is thus applied between $a_1 = 5$ cm and $a_2 = 10$ cm. To see the effect of the material variation we use the same conditions as in eqn (75).

7.2.1 Results stented artery

We take everything to be the same as in the standard artery test case. Again we compare our results with the results from [1] using the discontinuous Galerkin method. In figure 8 the pressure waves are shown.

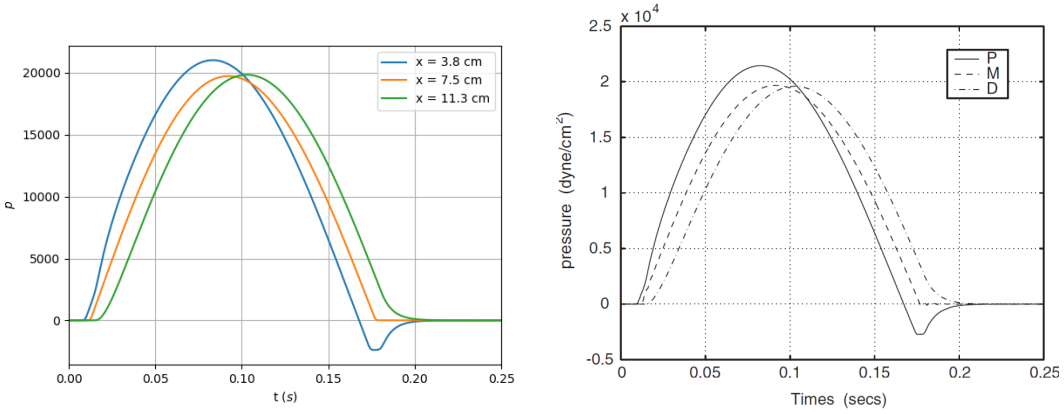

(a) Results of the stented artery in our model

(b) Results of the stented artery from Sherwin et al. [1]

Figure 8: Results of the test case of a stented artery. Subfigure (a) shows our results, and subfigure (b) is from Sherwin et al. In both cases, the pressure wave is plotted at $\frac{1}{4}$L, $\frac{1}{2}$L and $\frac{3}{4}$L.

We note that again our results and the results from Sherwin are very similar. Although there are minor differences, both approaches yield consistent outcomes. What is more interesting is the effect of adding a stent on the pressure wave. We recall, $\lambda_1 \propto \beta$ so inside the stent, the wave is traveling a bit faster. Thus the points M and D (figure 7) are reached a bit earlier than in the non-stented case. This effect is seen when comparing figure 6 and 8. In this test case, we can differentiate three distinct regions: before the stent, after the stent, and inside the stent. Inside each part, the material properties are constant so the solution is fully described by eqn (31). So here we expect to see non-distorted wave propagation similar to figure 6. On the other hand, there is a discontinuity in the material properties at the border of these parts. At the left boundary of the stent, we have an increase in β. This creates a partly positive reflected wave and a transmitted wave. The reflected wave reaches point P around 0.015 s and creates an increase in the pressure wave. At the right boundary, we have a decrease in β which results in a negative reflected wave. So the first transmitted wave now generates a negative reflected wave. This wave reaches point P around 0.17 s. This effect is visible in figure 8. Note that in principle each time a wave reaches one of the borders of the stent, part of the wave is reflected and part of the wave is transmitted. The result is that the energy is trapped in the stent and gradually dissipates through transmitted waves. This continuous process of transmission and reflection also accounts for most of the other differences between the stented pressure waves and the waves from figure 6. Lastly, we must note that having such a sharp discontinuity in the domain may create problems numerically. To reduce the negative effects we have ensured that the boundary of a grid cell coincides with the boundary of the stent.

These two test cases have learned us about how the numerical scheme of eqn (63) works and how it is implemented. Furthermore, it has shown us the effects of material variations on the solution. Sherwin did one extra test case, the case of a tapered artery. The implementation of this test case using our model can be found in the appendix.

8 Concentration

In the previous chapters, we have focused on eqn (17). This system describes the course of the velocity and cross-sectional area in the human blood system. In this work, the goal is to add the propagation of a chemical species in this system. To start this, we have seen the equation which describes the propagation (eqn (16)). This equation is known as the *advection-diffusion equation*. In this chapter, we look at the implementation of the concentration in arteries.

8.1 Numerical method

We aim to simulate the propagation of a species in the circulatory system. For that, we need numerical tools to implement eqn (16). Similar to what was done in chapter 5, we try to find a numerical difference scheme. Note that the advection-diffusion equation consists of three parts $\frac{\partial c(x,t)}{\partial t}$, $D\frac{\partial^2 c(x,t)}{\partial x}$ and $U(x,t)\frac{\partial c(x,t)}{\partial x}$. We will approximate the derivatives using the finite-difference method. In the appendix, this choice of numerical method is discussed in more detail. With the choice of finite difference, we subdivide the domain into intervals of length Δx. We (re)define $c_i^n = c(i\Delta x, t^n)$ and $U_i^n = U(i\Delta x, t^n)$ so it denotes the concentration and velocity in each subinterval respectively. With this, we follow Vuik et al.[10] to reach the following scheme

$$c_i^{n+1} = c_i^n - \frac{U_i^n \Delta t}{2\Delta x}(c_{i+1}^n - c_{i-1}^n) + D\frac{\Delta t}{\Delta x^2}(c_{i+1}^n - 2c_i^n + c_{i-1}^n) \tag{77}$$

Here we have approximated the first- and second-order spatial derivatives with first- and second-order central differences respectively. For time integration we use *Forward Euler*.

8.1.1 Stability

The Forward Euler method is only conditionally stable. It is therefore important to determine the size of the time step such that we ensure stability. Please see [20] for the derivation of the stability condition which we will take here without justification. For stability in the diffusion part, we need to ensure that

$$\frac{D\Delta t}{\Delta x^2} \leq \frac{1}{2} \tag{78}$$

Similarly, for the advection part we need to ensure that

$$-2 \leq \mathrm{P}_c = \frac{U\Delta x}{D} \leq 2 \tag{79}$$

P_c can be seen as the Péclet number of the cell. Note that these conditions implicitly ensure that the CFL condition is satisfied.

8.2 Test case 1

To verify our numerical method we consider a standard artery of finite length L and cross-sectional area A_0. At the start of the artery, we inject a chemical species with a concentration of c_0. We only inject this specimen for a finite time. In addition, we assume the blood in the artery has a constant velocity of v and a constant diffusion coefficient D. Figure 9 shows a representation of this test case. As mentioned earlier, we assume that the injected chemical species does not affect the blood dynamics in any way.

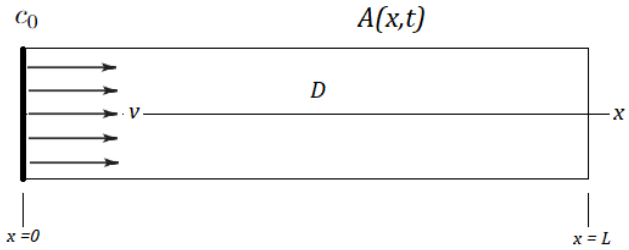

Figure 9: A schematic representation of the artery from the concentration test case.

We take $v = 0.5$ m/s, $D = 0.0005$ m^2/s and $L = 0.3$ m. During $t_0 = 0.033$ s we inject a concentration of $c_0 = 1$ kg/m^3. So the problem can be written as follows

$$\text{IC: } c(x,0) = 0, \quad \text{BC1: } c(0,t) = \begin{cases} c_0 & t < t_0 \\ 0 & t > t_0 \end{cases}, \text{BC2: } \frac{\partial c}{\partial x}(L,t) = 0 \tag{80}$$

Our numerical results are compared with the analytical solution to this problem. We follow [21] for the analytical solution to this problem. Figure 10 shows the result of this test case.

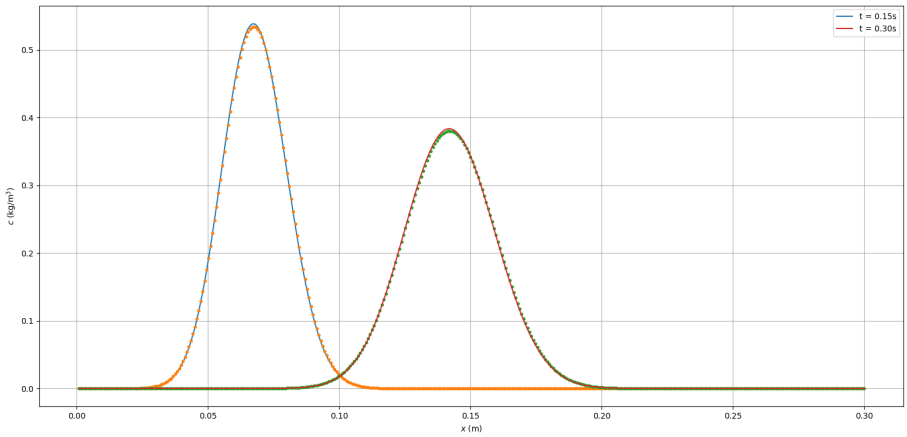

Figure 10: A plot of the numerical and analytical computed solution of the test case. The concentration is shown at $t = 0.15$s (the first peak) and $t = 0.30$s (the second peak). The dots represent the analytical solution while the continuous line represents the numerically computed solution.

We first consider the behaviour of the solution. Initially, we applied a square pulse input with a duration of t_0. By examining the evolution of the wave at $t = 0.15$ s, we can observe that it has propagated a distance of $x = 0.075$ m. This propagation can be understood by recalling that the solution follows an advection-diffusion equation. Hence, the observed movement is a consequence of the advection component of the equation. Considering we expect the wave to travel with a velocity of $v = 0.5$ m/s, then after 0.15 s, we expect the *middle* of the square pulse to have a displacement of $\Delta x = v(\Delta t - \frac{t_0}{2}) = 0.067$

m. This is indeed the case as seen in the figure. The next thing which can be noted is that the wave does not have the shape of the square pulse anymore, it is smeared out. Consequently, we see that the height of the peak is not at $c_0 = 1$ kg/m^3 as we would expect with pure advection. Again this is not surprising. The diffusive part of the equation accounts for the 'smearing out' of the solution. This diffusive process is continued as the wave propagates through the artery. Therefore, the concentration at $t = 0.30$ s is again much more diffused. From this test case, we see that any concentration of chemical species is slowly decreasing as it is propagating through the blood system. Lastly, we compare the numerical solution with the analytical solution. The two solutions are highly comparable, with the only noticeable difference occurring at the peak of the concentration wave. This discrepancy is likely a numerical error which can be accepted because it is very small. In summary, we have observed that our numerical scheme yields expected results for the case of constant velocity. However, it is important to note that the velocity is not constant when considering concentration propagation in the human circulatory system. For a test case involving an artery with a non-constant velocity we refer to the appendix.

9 Modeling the circulatory system

In previous chapters we have worked on building a model for describing the concentration propagation. We have derived methods that enabled us to implement these models. Before we can start analysing this propagation, we first discuss some important properties of the human system. These include modeling the heart, treatment of bifurcations, and modeling capillaries.

9.1 Modeling the heart

The human heart is the driving force in the system and so it is in our model. There are various approaches to model the heart. In previous works like [22] they have developed a very realistic way to model the heart using the filling and draining of the individual heart chambers. In our work, we use a much simpler approach following [1, 7]. We assume the contraction of the heart generates a pressure pulse. At his turn, the pressure wave forces the cross-sectional area of the adjacent artery to increase. This expansion in the first artery is then modeled as an inflow condition.

$$A_{bc}(t) = A_0 + 1.587 \cdot \alpha(t) H(\alpha(t)) \quad \alpha(t) = \sin(2\pi t + 0.628) - 0.588 \tag{81}$$

Note that $H(t)$ is again the Heaviside function [23]. In the figure below, a sketch of the inflow condition is seen. We see that at each beat the cross-sectional area of the adjacent artery is increased by 10%. For our second boundary condition we, as said in the *forward prescribing* section, fix s_2 at its initial value. Moreover, note that this model has a heart rate of around 60 bpm. Which is a normal rate at rest.

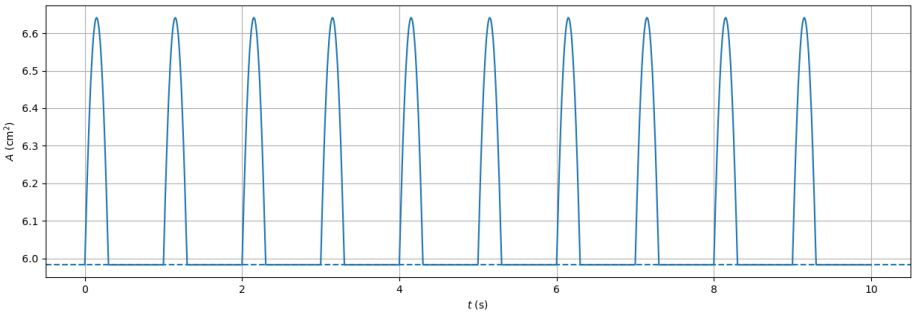

Figure 11: A plot of the inflow boundary condition which models the heart rate (eqn (81))

9.2 Treatment of bifurcations

The human arterial tree is over 90.000 km in length but no artery is longer than 45 cm. This is caused by all the bifurcations in the system. A bifurcation occurs if one parent vessel is branched into daughter vessels. In figure 12 a scheme of such a bifurcation is shown. In reality, there also exists trifurcations and more complex bifurcations. In this model, we do not consider those and model all the bifurcations similarly. In our numerical computation, we treat each artery separately but use the information from the characteristics to define boundary conditions for the parent and his daughters. Note that at a bifurcation there is often a discontinuity in A and in β. However, we still force that there is a conservation of the characteristic variables, pressure, and mass. Furthermore, we expect concentration to have a smooth transition at the bifurcation. These seem like realistic assumptions which will prove itself useful. Note that we have 9 unknown values at a bifurcation (also indicated in the figure). However, we can simplify

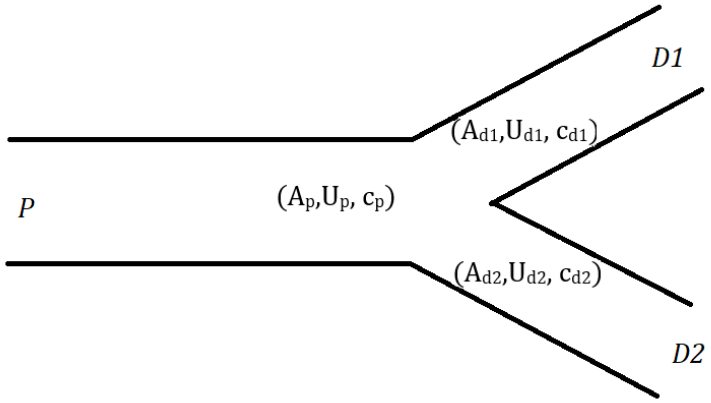

Figure 12: Schematic representation of a bifurcation. The P symbolizes the parent vessel and $D1$ and $D2$ the two daughter vessels

things by noting that the concentration should be continuous across the bifurcation. So that means that for the concentration we can just 'ignore' the branching since it does not affect the value of the concentration. At the bifurcation we write eqn (77) as

$$c_p^{n+1} = c_p^n - \frac{U_p^n \Delta t}{2\Delta x}(c_d^n - c_{p-1}^n) + D\frac{\Delta t}{\Delta x^2}(c_d^n - 2c_p^n + c_{p-1}^n) \tag{82}$$

Where c_p denotes the concentration at the last parent cell and c_d at the first daughter cell. Note that concentration in both daughters is similar in the first cell of their vessel. This is due to the continuity condition. Moreover, note that a similar approach can be applied to c_d^{n+1}. With this, only 6 unknowns remain. So, our goal is now to find 6 equations to solve for the velocity and cross-sectional area. The first three can be found using the characteristic variables so

$$s_{1_p} = U_p + 4A_p^{\frac{1}{4}}\sqrt{\frac{\beta_p}{2\rho}}, \quad s_{2_{d_j}} = U_{d_j} - 4A_{d_j}^{\frac{1}{4}}\sqrt{\frac{\beta_{d_j}}{2\rho}} \tag{83}$$

We have denoted d_j as daughter j. The next three equations come from the conservation laws. First the conservation of mass

$$A_p U_p = A_{d_1} U_{d_1} + A_{d_2} U_{d_2} \tag{84}$$

Next, we expect no discontinuity in pressure

$$\frac{\rho U_p^2}{2} + p_{ext(p)} + \beta_p\left(\sqrt{A_p} - \sqrt{A_{0_p}}\right) = \frac{\rho U_{d_j}^2}{2} + p_{ext(d_j)} + \beta_{d_j}\left(\sqrt{A_{d_j}} - \sqrt{A_{0_{d_j}}}\right) \tag{85}$$

Eqns (83 84 85) can be written in the following form

$$f_1 = s_{1_p} - U_p - 4A_p^{\frac{1}{4}}\sqrt{\frac{\beta_p}{2\rho}} = 0 \tag{86}$$

$$f_2 = s_{2_{d_1}} - U_{d_1} + 4A_{d_1}^{\frac{1}{4}}\sqrt{\frac{\beta_{d_1}}{2\rho}} = 0 \tag{87}$$

$$f_3 = s_{2_{d_2}} - U_{d_2} + 4A_{d_2}^{\frac{1}{4}}\sqrt{\frac{\beta_{d_2}}{2\rho}} = 0 \tag{88}$$

$$f_4 = A_pU_p - A_{d_1}U_{d_1} - A_{d_2}U_{d_2} = 0 \tag{89}$$

$$f_5 = \frac{\rho U_p^2}{2} + p_{ext(p)} + \beta_p\left(\sqrt{A_p} - \sqrt{A_{0_p}}\right) - \frac{\rho U_{d_1}^2}{2} - p_{ext(d_1)} - \beta_{d_1}\left(\sqrt{A_{d_1}} - \sqrt{A_{0_{d_1}}}\right) = 0 \tag{90}$$

$$f_6 = \frac{\rho U_p^2}{2} + p_{ext(p)} + \beta_p\left(\sqrt{A_p} - \sqrt{A_{0_p}}\right) - \frac{\rho U_{d_2}^2}{2} - p_{ext(d_2)} - \beta_{d_2}\left(\sqrt{A_{d_2}} - \sqrt{A_{0_{d_2}}}\right) = 0 \tag{91}$$

We have now derived 6 equations with 6 unknowns. A popular method to solve this system is using the *Newton-Raphson method*. We write $\mathbf{x} = [A_pA_{d_1}A_{d_2}U_pU_{d_1}U_{d_2}]^T$. Following [10] we can write

$$\mathbf{x}^{(k)} = \mathbf{x}^{(k-1)} - \mathbf{J}^{-1}(\mathbf{x}^{(k-1)})\mathbf{f}(\mathbf{x}^{(k-1)}) \tag{92}$$

Here $\mathbf{f} = [f_1 f_2 \cdots f_6]^T$ and $\mathbf{J}$ is the Jacobian matrix of $\mathbf{f}(\mathbf{x})$

$$\mathbf{J}(\mathbf{x}) = \begin{bmatrix} \frac{\partial f_1}{\partial A_p} & \cdots & \frac{\partial f_1}{\partial U_{d_2}} \\ \vdots & \ddots & \vdots \\ \frac{\partial f_6}{\partial A_p} & \cdots & \frac{\partial f_6}{\partial U_{d_2}} \end{bmatrix} \tag{93}$$

Note that eqn (92) is an iterative function so as a stopping condition we enforce that $|\mathbf{x}^{(k-1)} - \mathbf{x}^{(k)}| \leq \epsilon$ with $\epsilon = 0.01$.

9.2.1 Test case bifurcation

Above, we have derived a method of how to treat the bifurcation in the circulatory system. We test our method in the following setting. We consider a parent-daughter pair similar to the one illustrated in figure 12. We again inject a chemical species with a concentration of $c_0 = 1$ g/cm^3 $t_0 = 0.01$ seconds long at the start of the parent vessel. To make sure that the concentration wave reaches the daughter in $T = 0.1$ seconds we take each of the three arteries only to be $L = 1$ cm. We assume

$$A(0,t) = A_0 + 0.35|\sin\frac{4\pi t}{T}| \tag{94}$$

Furthermore, we consider the symmetrical case which means the properties of both daughters are identical. $A_p = 6$ cm^2, $A_{d_1} = A_{d_2} = 3$ cm^2. $\beta_p = 1 \cdot 10^5$ dyne/cm^3 and $\beta_{d_1} = \beta_{d_2} = 1.5 \cdot 10^5$ dyne/cm^3.

We also want to investigate the effect of the bifurcations on pressure. To that end, we consider how a pressure wave propagates through the bifurcation. It is important to mention that if we use the test case for the concentration above to analyse the pressure, no viable wave appears. This is due to the periodicity and the amplitude of the input function. To that extent, we slightly change the situation to a case in which the arteries are each $L = 3$ cm long, and the inflow boundary is given as

$$A(0,t) = A_0 + e^{-10^6(t-0.01)^2} \tag{95}$$

Below, the test results are shown in figure 13. Each of the two plots can be subdivided into three parts. The first part (until $x = 3$ cm) represents the parent domain, the second part ($x = 3$ cm until $x = 6$ cm) represents the domain of daughter 1, and the final part represents the domain of daughter 2. We first analyse the propagation of the pressure wave. We note that similar to the test cases performed earlier (see chapter 7), the wave is gradually advecting through the domain. The wave reaches the bifurcation at $t = 0.018$s from where it travels symmetrically in the two daughter domains. This symmetry in both daughter domains is expected, as the material properties are similar in both cases. Furthermore, we note that there is no reflective wave at the bifurcation. In the stented artery test case, we observed that when a pressure wave encounters a discontinuous increase in β, it generates a negative reflective wave. However, we now do not see a negative reflective wave despite the discontinuous increase in β. This can be understood by realising there is also a discontinuous decrease in A at the bifurcation. The discontinuity might give rise to a positive reflective wave which exactly cancels with the negative reflected wave caused by the increase in β.

Next, we look at the concentration profile. We immediately notice the expected advective and diffusive behaviour. Moreover, we see a continuous behaviour with no jump at the bifurcation. In addition, we note the symmetry in the two daughter parts which is again as desired.

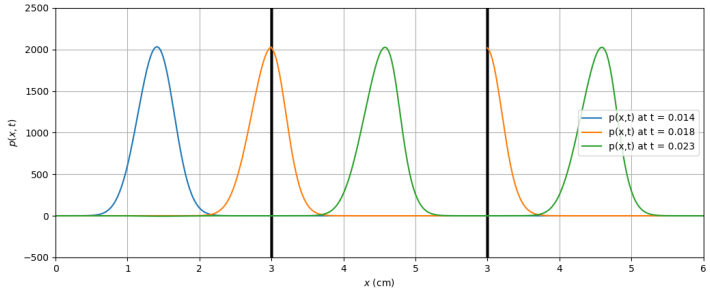

(a)

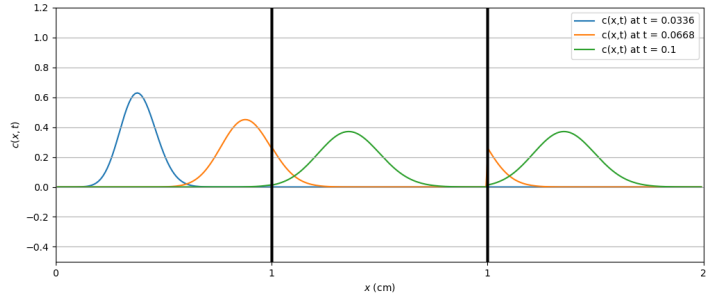

(b)

Figure 13: Numerical results of the bifurcation test case. Both plots are subdivided into three parts. The first part shows the parent's domain, the second part shows the domain of daughter 1 and the last part shows the domain of daughter 2. (a) Shows the propagation of the pressure wave in the parent-daughter system. The pressure wave is plotted at $t = 0.014$s, $t = 0.018$s, and $t = 0.024$s. (b) Shows the propagation of the concentration wave. The wave is plotted at $t = 0.033$s, $t = 0.066$s, and $t = 0.1$s.

Lastly, we test the asymmetric case. Now, the cross-sectional areas of the daughters are made different. In addition, we equal the stiffness (β) of the parent and its daughters. In this way, we hope to see the influence of β. We now also expect to see differences in velocity between the two daughters because the cross-sections are different but the total mass flowing through the bifurcation must still be equal (note that this is captured in eqn (84)). We take $\beta_p = \beta_{d_1} = \beta_{d_2} = 1.5 \cdot 10^5$ dyne/cm^3 and $A_p = A_{d_1} = \frac{1}{2}A_{d_2} = 6$ cm^2. The results are shown in figure 12.

Note that we now have an asymmetrical behaviour. We clearly see the difference between daughter 1 and daughter 2 as expected. There is indeed a difference in velocity between the daughters. This is expected as the total volume flux (UA) is constant. So a smaller A results in a higher U in daughter 2. We moreover see that the concentration wave has propagated a bigger distance in the parent compared to our previous test case. This could have been expected as $c = \sqrt{\frac{\beta}{2\rho}}A^{\frac{1}{4}}$, so an increase in β means an increase in the velocity. Please consider [7, 8] for an analysis of the asymmetric bifurcation test case regarding the pressure wave.

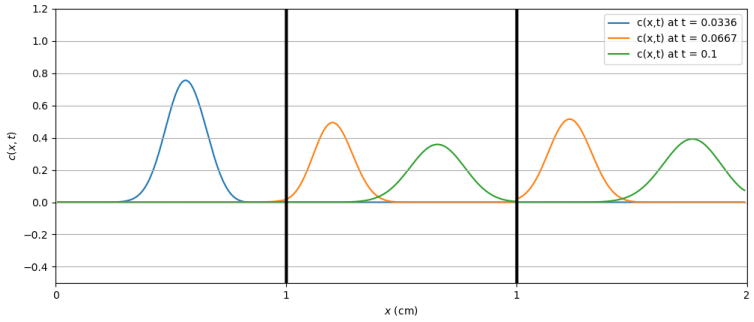

Figure 14: A plot of the parent-daughter test case with $A_p = A_{d_1} = \frac{1}{2}A_{d_2}$ and $\beta_p = \beta_{d_1} = \beta_{d_2}$. The plot can be subdivided into three parts. The first part shows the parent's domain, the second part shows the domain of daughter 1 and the last part shows the domain of daughter 2.

9.3 Terminal arteries

The number of branches dramatically increases towards the end of the arterial tree. All these capillaries cannot be modeled individually but researchers have found a way to model their combined effect. To this end, the effect of these capillaries will creates boundary conditions for the terminal arteries. Following [4] we assume these effects are purely resistive. To that extent, we define the reflection coefficient R_t

$$R_t = -\frac{\Delta s_2}{\Delta s_1} = -\frac{s_2^{n+1} - s_2^0}{s_1^{n+1} - s_1^0} \approx -\frac{s_2^n - s_2^0}{s_1^n - s_1^0} \tag{96}$$

Then solving for s_2^n we get

$$s_2^n = s_2^0 - R_t(s_1^n - s_1^0) \tag{97}$$

Even though this is quite a simple approach, it has proven itself to be sufficiently accurate for our goals. Note that a reflective coefficient of 1 means total reflection while a coefficient of 0 accounts for an open end.

10 The human arterial tree

We finally have all needed materials to implement our system in the human arterial tree. We consider a system of the 55 main arteries. This model excludes the brain and some smaller arteries in the torso. This model of arteries is also used in [1, 8]. Below is an overview of the arterial tree.

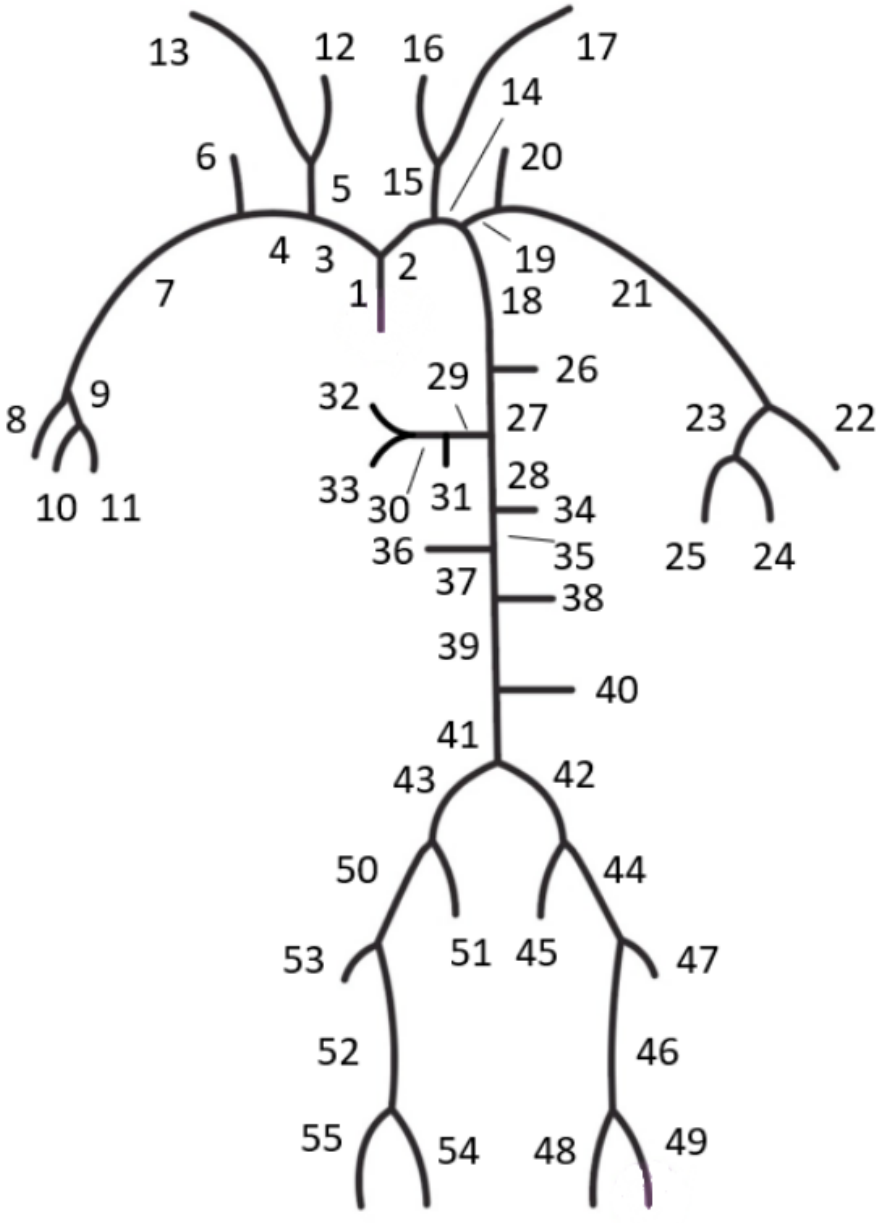

Figure 15: An overview of the arterial tree used in this work from [7].

It is preferable to use this model as the values of β, A_0, and R_t as experimentally determined and listed for these 55 arteries. The physiological data is listed in the appendix.

Our model can be seen as a composition of two. One model for the velocity and area, and the one for the concentration. But remember that the concentration model is highly dependent on the velocity. For the model describing the velocity and cross-sectional area, we use the boundary conditions as described in chapter 9. For the concentration model, we again use an injection boundary and a free outflow boundary. Hence we have

$$\text{IC: } \begin{bmatrix} A \\ U \end{bmatrix} = \begin{bmatrix} A_0 \\ 0 \end{bmatrix} \quad \text{BC1: } A(0,t) = A_{bc}(t) \quad \text{BC2: } s_2(L,t) = s_2(0,t) - R_t\left[s_1(L,t) - s_1(0,t)\right] \tag{98}$$

and

$$\text{IC: } c(x,0) = 0 \quad \text{BC1: } c(0,t) = \begin{cases} c_0 & t < t_0 \\ 0 & t > t_0 \end{cases} \quad \text{BC2: } \frac{\partial c}{\partial x}(L,t) \tag{99}$$

We compare the velocity and cross-sectional area with the work of Sherwin[1]. Below we plot the velocity and cross-sectional area of artery 1 and artery 49 (see figure 15). It is plotted for 1 second once it is fully developed. In this model $\rho = 1.06$ g/cm^3 and $p_{ext} = 0$ dyne/cm^2.

Figure 16 and 17 show our result at two different arteries. Here, the $R_t = 0$ for every terminal artery. So in this model, we have not yet added reflection and friction. For an analysis with the addition of these two factors, we refer to the appendix. We first note that the results of both arteries are very similar to the literature. We have chosen artery 49 since it is almost at the end of the tree, in the leg. If any error occurred previously, it would propagate and amplify through the system and thus be visible at the end. So figure 17 convinces us that no major error occurred earlier in the tree. Remember that s_2 is the left traveling wave. In two perfectly matching arteries, we would not expect an s_2-wave to occur. This is because there is no reflection at the bifurcation and no terminal reflection. This is for example seen in figure 17. Note that artery 1 does have a (small) back traveling wave. This is because the adjacent arteries do not fully match and the forward traveling wave creates a reflective wave (similar to our stented test case) which is seen as a s_2-wave. Note that in artery 1, the cross-sectional area increases according to s_1. This is not surprising as we have used forward prescribing (see section *forward prescribing* in chapter 6). Moreover, we note that the general shape of the velocity and cross-sectional area is similar to the inflow condition (see figure 11). So again the inflow condition is propagating through the system. Lastly, note that the results look physically possible. An expansion of 10% in the cross-sectional area seems reasonable for example. As well as the fact that the velocity in the arteries behaves wave-like. A velocity of 30 cm/s during systole seems high but reasonable. We must not forget that the velocity depends on other factors such as temperature and the exact geometry of the vessel. That is why it is difficult to compare the results with medical data from arteries, our model is too simplistic for that.

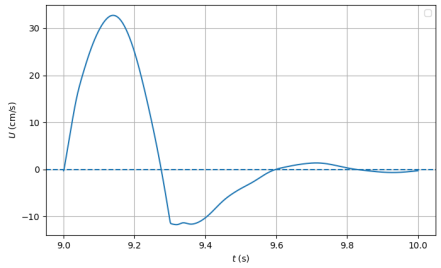

(a) The velocity in artery 1 with our model

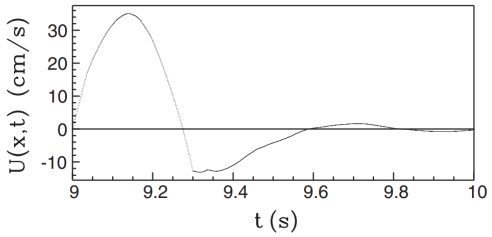

(b) The velocity in artery 1 from [1]

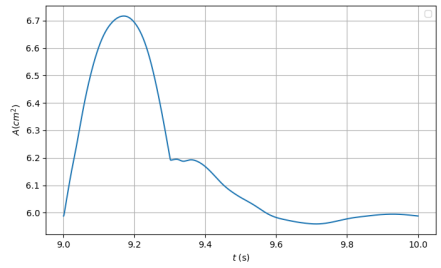

(c) The cross-sectional area in artery 1 with our model

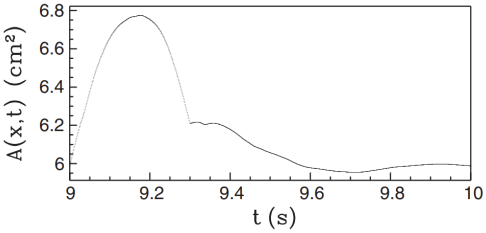

(d) The cross-sectional area in artery 1 from [1]

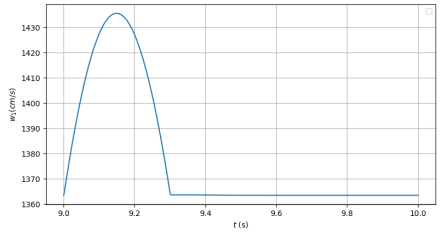

(e) The characteristic variable s_1 with our model

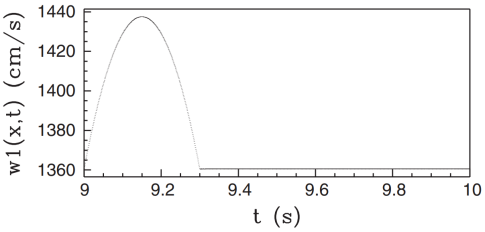

(f) The characteristic variable s_1 from [1]

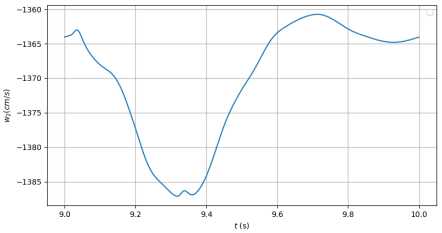

(g) The characteristic variable s_2 with our model

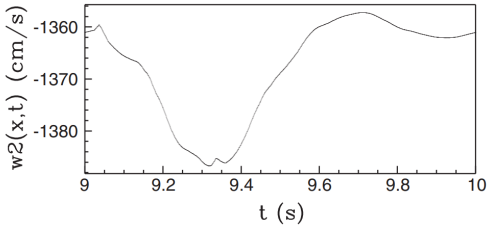

(h) The characteristic variable s_2 from [1]

Figure 16: The results of artery 1 of our model together with the literature results from [1]. From top to bottom, the velocity, cross-sectional area, and characteristic variables s_1 and s_2 are plotted respectively. The left column are our results and the right column is from [1].

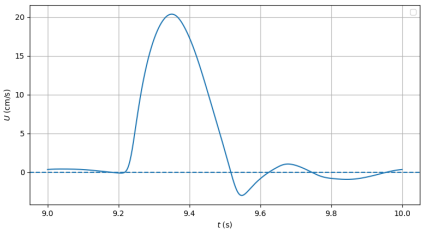

(a) The velocity in artery 49 with our model

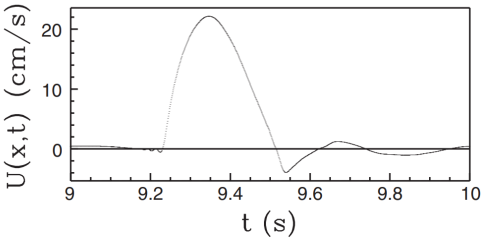

(b) The velocity in artery 49 from [1]

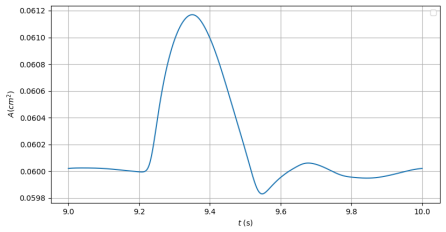

(c) The cross-sectional area in artery 49 with our model

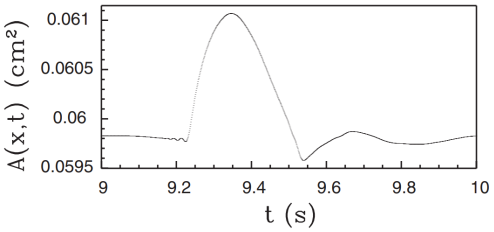

(d) The cross-sectional area in artery 49 from [1]

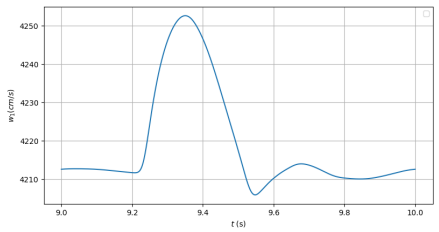

(e) The characteristic variable s_1 with our model

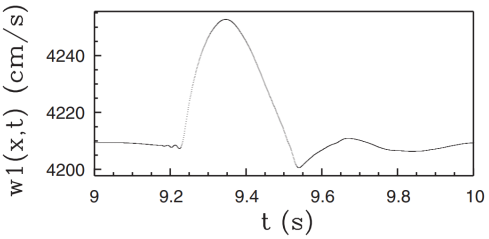

(f) The characteristic variable s_1 from [1]

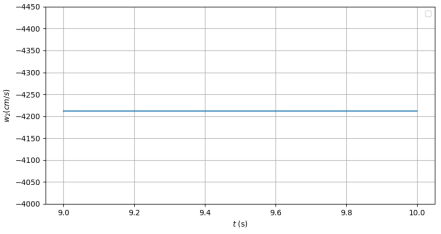

(g) The characteristic variable s_2 with our model

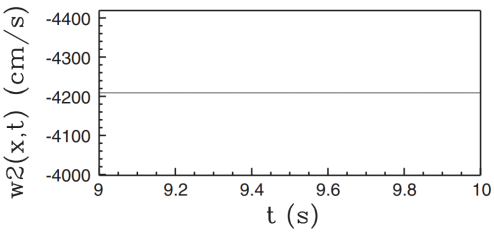

(h) The characteristic variable s_2 from [1]

Figure 17: The results of artery 49 of our model together with the literature results from [1]. From top to bottom, the velocity, cross-sectional area, and characteristic variables s_1 and s_2 are plotted respectively. The left column are our results and the right column is from [1].

To illustrate the propagation of velocity and pressure in the arterial tree, we have made a plot of the entire system. In the creation of this plot, the different arteries are represented as edges. These edges are assigned a color that represents their average velocity and pressure. Please note that the figure is not on scale (the exact lengths can be found in the appendix). Figure 19 nicely shows how the pressure is developing and propagating in the tree. At $t = 9.1$s the inflow boundary is starting to create a pressure wave. Indeed the velocity and pressure are the highest near the heart. As time moves on, the waves are propagating over the system and increase the pressure and velocity further in the tree. Moreover, note that in some places we have a negative velocity and pressure due to the reflective waves at the bifurcation. Lastly, we see that the velocity and pressure are low at $t = 9.7$s. This can be understood by realizing that one inflow cycle happens every 1 second. So at $t = 9.7$s, the inflow pulse from $t = 9$s has decayed, decreasing the pressure and velocity. A new cycle starts at $t = 10s$ increasing the velocity and pressure again. This means the profile at $t = 10.1$s would be very similar to that of $t = 9.1$s.

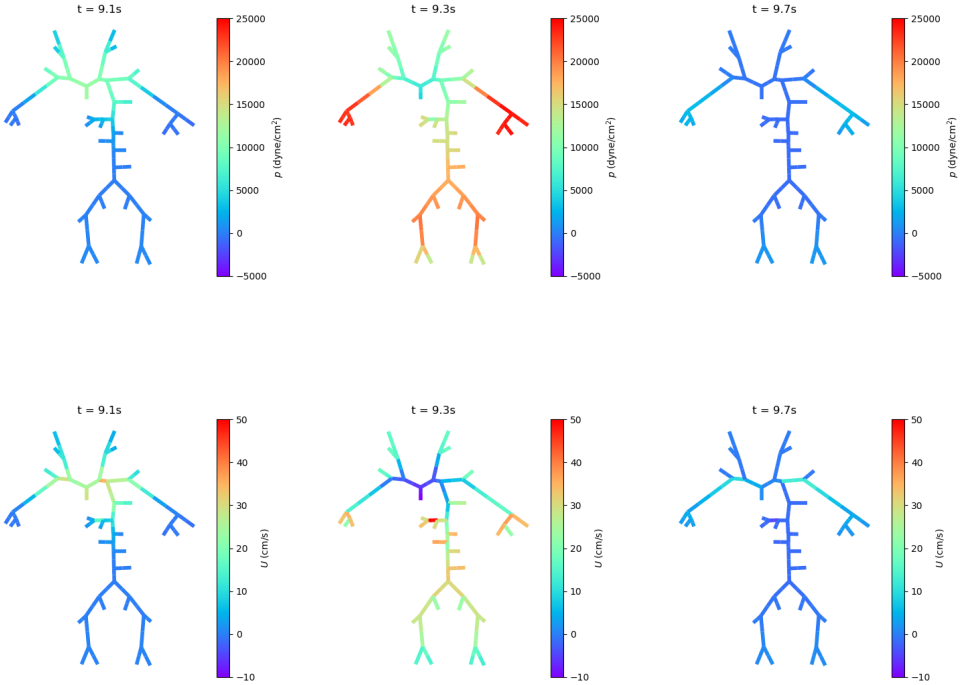

Figure 19: Visual representation of the velocity and pressure in the arterial tree. The upper row represents the pressure (p) and the lower row represents the velocity (U) inside the system. Three times are shown, $t = 9.1$s, $t = 9.3$s, and $t = 9.7$s.

It is now time to turn our attention to the concentration. During a period of $t_0 = 1$ second, we inject a concentration of $c_0 = 1$ g/cm^3. This concentration is injected in artery 1, so at the beginning of our model. We follow [3] and take $D = 0.2$ cm^2/s. With this said, note that we have just added the concentration of a chemical species to the previous model. Remember that we have a simple outflow terminal condition so there is no reflection of concentration of any kind. In figure 22 an overview of the way the concentration is propagating in the arterial tree is shown. The figure is created by dividing each artery into two edges. These edges are then colored based on the average concentration of the wave.

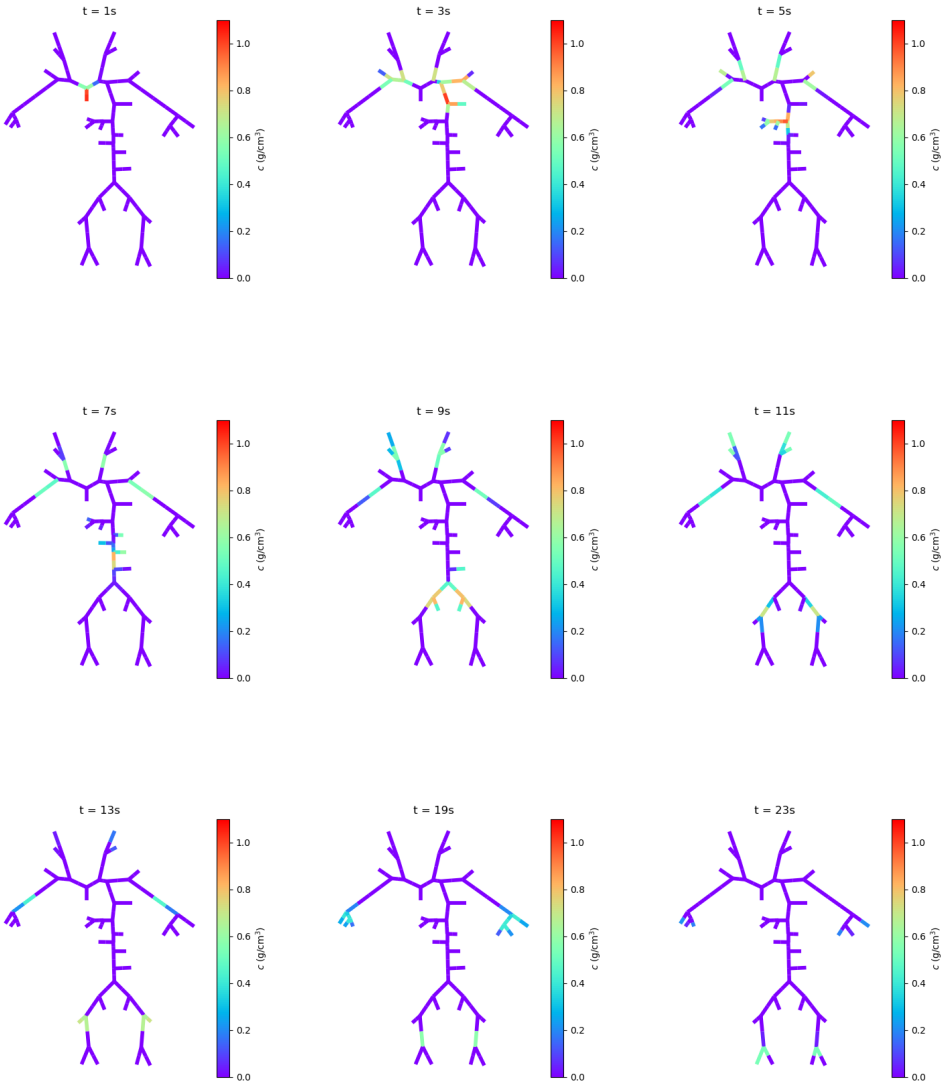

Figure 22: Visual representation of the propagation of a chemical species through the arterial tree with $D = 0.2\text{cm}^2/\text{s}$. The behaviour of the concentration profile is shown at 9 times.

We now take a closer look at what happens during the propagation. First note that we see the advection property in figure 22. Over time, the concentration wave is propagating in the tree. From figures 16 and 17 we have seen that the velocity at the end of the tree is around the 10% lower. This makes it so that we would expect a slightly lower advection rate near the end of the tree. Unfortunately, this is difficult to see since the representation is not on scale. Remember that if the relative velocity of the two branches at the bifurcation differs, this affects the concentration. If one branch has a higher velocity, more chemical species will advect to this branch. This can be seen in the figure as the concentration distribution at branches is not always uniform. The second property that can be seen in the plot is the diffusion property. We observe that the concentration becomes more diluted and spreads out over time. The peak of the

concentration wave which reaches the leg only is about 50% of its original value. So this shows that when injecting any chemical species into the body one should base the amount of concentration on the location where the substance needs to go. The longer the distance, the more diluted it becomes. We would also realise that the amount of chemical species decreases over the length of the tree. Even though the height of the peak is continuous at a bifurcation, the amount of volume flux is not. The volume flowing out of a parent should equal the sum of the volume flowing into the daughters. This then influences the amount of chemicals that reach a location.

Next, we take a more detailed look at the concentration profile in the different arteries. The concentration profiles are depicted in figure 23 and are taken at the beginning of the arteries. Firstly, it is important to note that the concentration slices do not accurately resemble the expected shapes. In the plot, small spurious oscillations can be seen which makes the interpretation of this profile harder. Moreover, the general shape of the wave does not resemble the waves we have seen in the test cases. The waves from figure 23 are more angular and less smooth. This is a weakness of this model. In our code, the information of the entire model is saved, resulting in a computationally heavy analysis. Consequently, not enough memory is available at the end of the process. Therefore, we are forced to choose a value for Δx that does not provide optimal accuracy. So, to optimize it, the modeling should be adjusted such that only information is required from the nearby arteries instead of the entire tree. Nevertheless, these plots give sufficient information to be able to say something about the average concentration and the propagation of the wave. In figure 23 we recognize the square pulse inflow condition in artery 1 and we note that once it has reached artery 49, the strength of the wave is greatly reduced. Also, note that the wave has broadened over time just as in our test case. In addition, remember that the velocity in the arterial tree moves like a wave. This means the velocity in an artery greatly increases for a short period of time after which the movement almost stops. For that reason, the average advection rate is way smaller than the amplitude of the velocity wave.

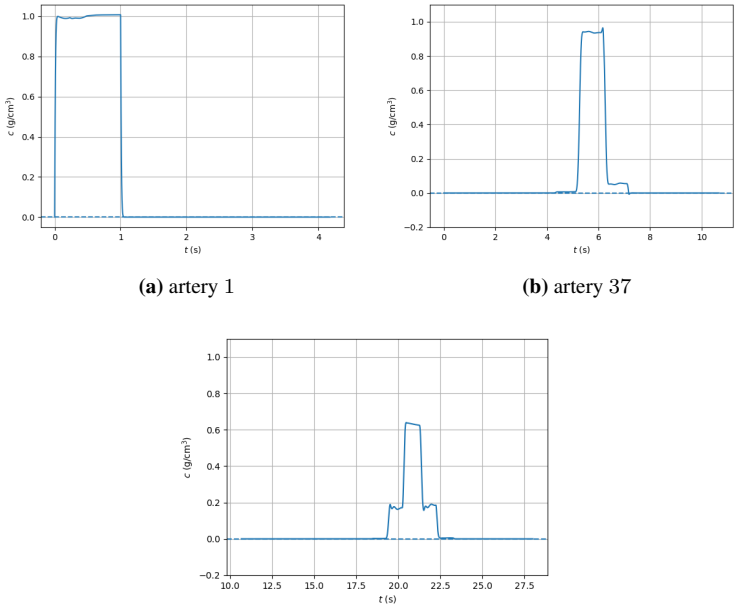

(a) artery 1 **(b)** artery 37

(c) artery 49

Figure 23: Result of the concentration profile in three different arteries with $D = 0.2$ cm^2/s and a 60 bpm heart rate

10.1 Concentration flow in running person

Next, we analyse the influence of the inflow condition on the concentration propagation. For that, we consider the situation in which a running person gets an injection (of course this is no realistic scenario). For that, we model a heart rate of 120 bpm which is an average running heart rate. In figure 25 the propagation through the body is shown.

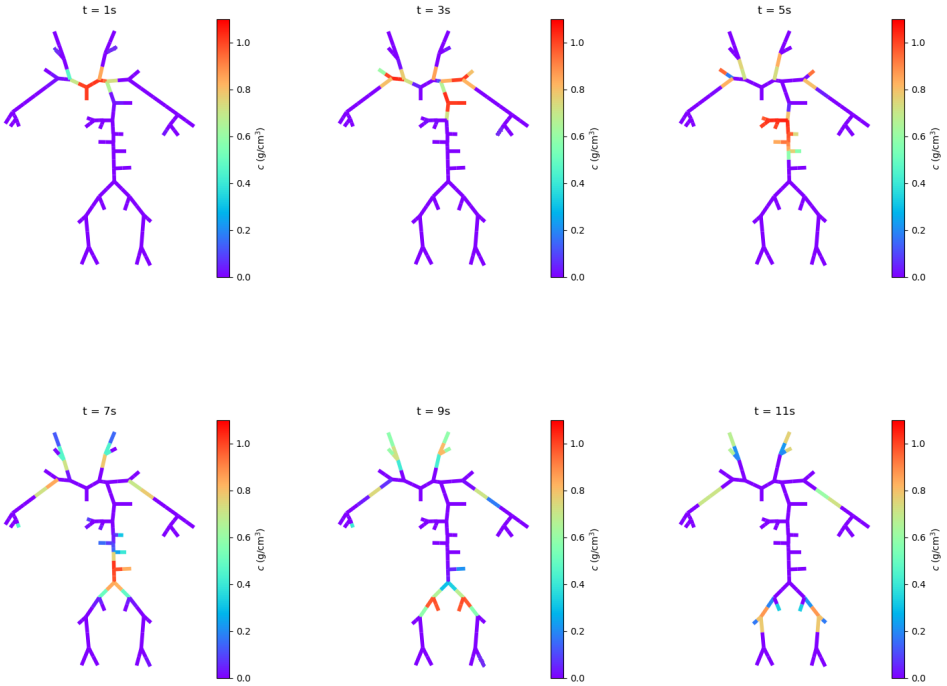

Figure 25: Visual representation of the propagation of a chemical species through the arterial tree with $D = 0.2$ cm^2/s and a heartbeat of 120 bpm. The behaviour of the concentration profile is shown at 6 times.

Please compare the above representation with the representation in figure 23. The heart rate in the running person is twice as big as in the previous model and thus we expect the concentration to propagate much faster. In the first case, a contraction of the heart occurs every second which means that velocity waves are generated each second. If this heart rate is doubled, a contraction occurs every 0.5s creating velocity waves faster after each other. The blood's velocity will then decrease less after such a wave passed since a new one is already coming. We indeed see a faster advection rate of the concentration in the plot. For example, note that at the $t = 5$s plot the concentration wave in figure 23 has reached artery 28 while with a heart rate twice as big, it reaches artery 37 after 5s. Suppose we want a chemical species to reach the legs, we see that a 60 bpm heart rate makes it so this takes around the $t = 20$ s but increasing the heart rate to 120 bpm reduces this time to around the $t = 15$ s. Furthermore, we see that the height of the concentration wave is higher when the heart rate is increased because it is less diluted. This could be expected. The diffusion coefficient is similar in both cases but since less time has passed before the wave reaches an artery, less time there was to dilute.

With this simulation, we can now understand that the velocity of the blood is very important in the transportation of a chemical species. Not only does it determine the time needed to reach a certain artery but also the level of concentration at which it reaches it. Altogether, it seems more effective to inject somebody who is running (or at least someone with a higher heart rate).

10.2 Influence of the diffusion coefficient

In the previous two simulations, we worked with a diffusion coefficient of $D = 0.2$ cm^2/s. In fact, the diffusion coefficient is a very complicated parameter that depends on for example the temperature, the viscosity of the blood, and the chemical species we are considering. For a more realistic model, D should thus be place and time-dependent. Because of all these dependencies, the diffusion coefficient is very difficult to estimate. That is why in this section we analyse the influence of changing the diffusion coefficient. We consider the cases $D = 2$ cm^2/s, $D = 0.2$ cm^2/s and $D = 0.02$ cm^2/s.

With these choices of D, we might run into trouble with the stability criterium of the central difference method (CDM) (see eqn (79)). To ensure a more stable result we use the central difference method in combination with *Beam-Warming Method*. At each time step we determine the local Péclet number. If eqn (79) is satisfied we use the more accurate CDM and otherwise switch to BWM. In the appendix, we have already shown that the BWM works just as well as the CDM in the test cases. That is why we can easily interchange these two.

In figure 28, the results of the concentration wave in arteries 37, 43, and 51 are presented for simulations with diffusion coefficients of $D = 0.02$ cm^2/s, $D = 0.2$ cm^2/s, and $D = 2$ cm^2/s. It is important to note that these plots provide an overall understanding of the wave's behavior and its average value, rather than precise details.

We consider the different cases. In case (III), the plots closely resemble the waves observed in the test cases. This occurs because the Péclet number remains mostly below 2, allowing the CDM to provide relatively accurate results. It is evident that the waves become more diluted compared to cases (I) and (II), which aligns with our expectations as the higher diffusion coefficient induces greater diffusion in each time step. Suppose we want an injected drug to reach the leg, a diffusion coefficient of $D = 0.02$ cm^2/s retains about 85% of its original concentration, while $D = 2$ cm^2/s reduces it to 40%. So we see that knowledge about the diffusion coefficient is essential when injecting a medicine.

In the first two arteries, simulations (I) and (II) show minimal differences in dilution, despite the tenfold difference in diffusion coefficients. This may be attributed to their small coefficients and the short elapsed time. Therefore, no significant difference could yet have been made. Next, note that we see the waves get more diluted as they travel. This effect is visible no matter the value of D and is of course what we would expect. Lastly, note that the peak's position is independent of D. This is what we would expect as D only influences the level of dilution and not the velocity.

Regarding all the concentration plots, we again note small spurious oscillations. The inaccuracy of the results is partly due to the value of D. The stability region of our time-integration method (see [10] for more detail) is dependent on the value of D. The higher the value of D, the more accurate the results. Moreover, LeVeque [6] had shown that even though BWM greatly reduces numerical oscillations it does not eliminate them. That is why we also see oscillations in the simulations (just like in figure 23). In future research, a finer grid can be used to get waves that show more similarity with the test cases.

(I) $D = 0.02\ \text{cm}^2/\text{s}$

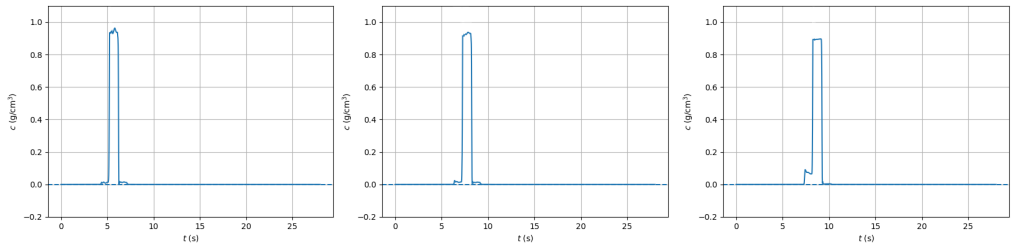

(II) $D = 0.2\ \text{cm}^2/\text{s}$

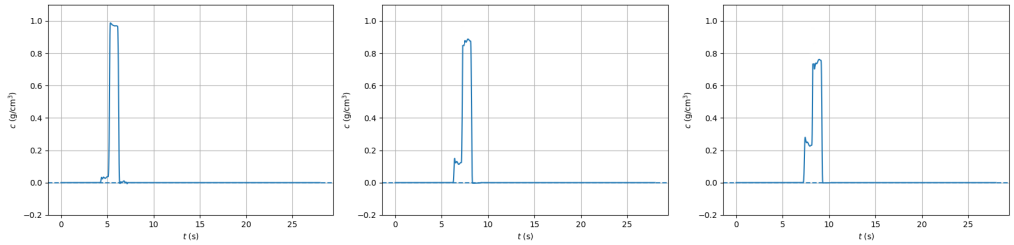

(III) $D = 2\ \text{cm}^2/\text{s}$

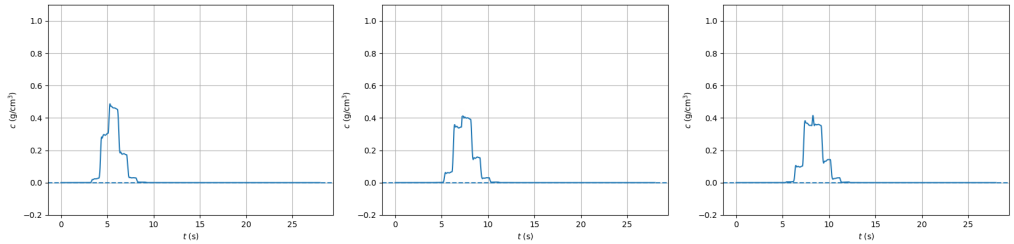

(a) artery 37 **(b)** artery 43 **(c)** artery 51

Figure 28: This plot shows the result of three arteries in three different simulations. The upper row shows the result when $D = 0.02\ \text{cm}^2/\text{s}$, the middle row when $D = 0.2\ \text{cm}^2/\text{s}$, and the last row when $D = 2\ \text{cm}^2/\text{s}$. In each of these three simulations, the concentration profile at the beginning of artery 37, 43, and 51 are shown respectively.

To get a nice overview of the propagation of the concentration in the arterial tree, we have again made a visual representation. Figure 32 shows how the waves are traveling through the system. Only the times $t = 3$s, $t = 5$s, $t = 7$s, and $t = 9$s are plotted as this gives enough information about the propagation. Note that from this figure it is clear that $D = 2$ cm^2/s creates much more diluted waves. The value of the concentration is a lot lower than in the other two cases. Moreover, note that the waves are also more spread out in comparison with the other two. At $t = 7$s, the concentration wave has partly reached artery 42 in the first simulation but this is not the case in the other two. Please remember that figure 32 is not on scale and each artery is modeled as an edge which is colored based on its average value. Because of this, the broadening of the wave is not visible at the $t = 9$s plot. The arteries here are just a lot longer. So, this broadening and lowering of the height is indeed what we would expect for a higher diffusion coefficient. Moreover, there is also a difference between the $D = 0.2$ cm^2/s and the $D = 0.02$ cm^2/s even though this one is less obvious. As time moves, we note a difference in value between these two. At $t = 7$s, there is a clear value difference in artery 39. Note that it does not seem like the waves from the second simulation are much broader than those in the third. Apparently the smearing out is not as big as the length of the edges.

To summarize, this analysis of the diffusion coefficient had shown us that our model behaves as expected no matter the value of D. It has also shown that the accuracy of the concentration plots is dependent on the Péclet number (and thus D) and that spurious oscillations can occur in our model. This model should therefore just be used to give an indication of the diffusivity and velocity of concentration propagation in the human body. It is not accurate enough to say something about the precise nature of the wave.

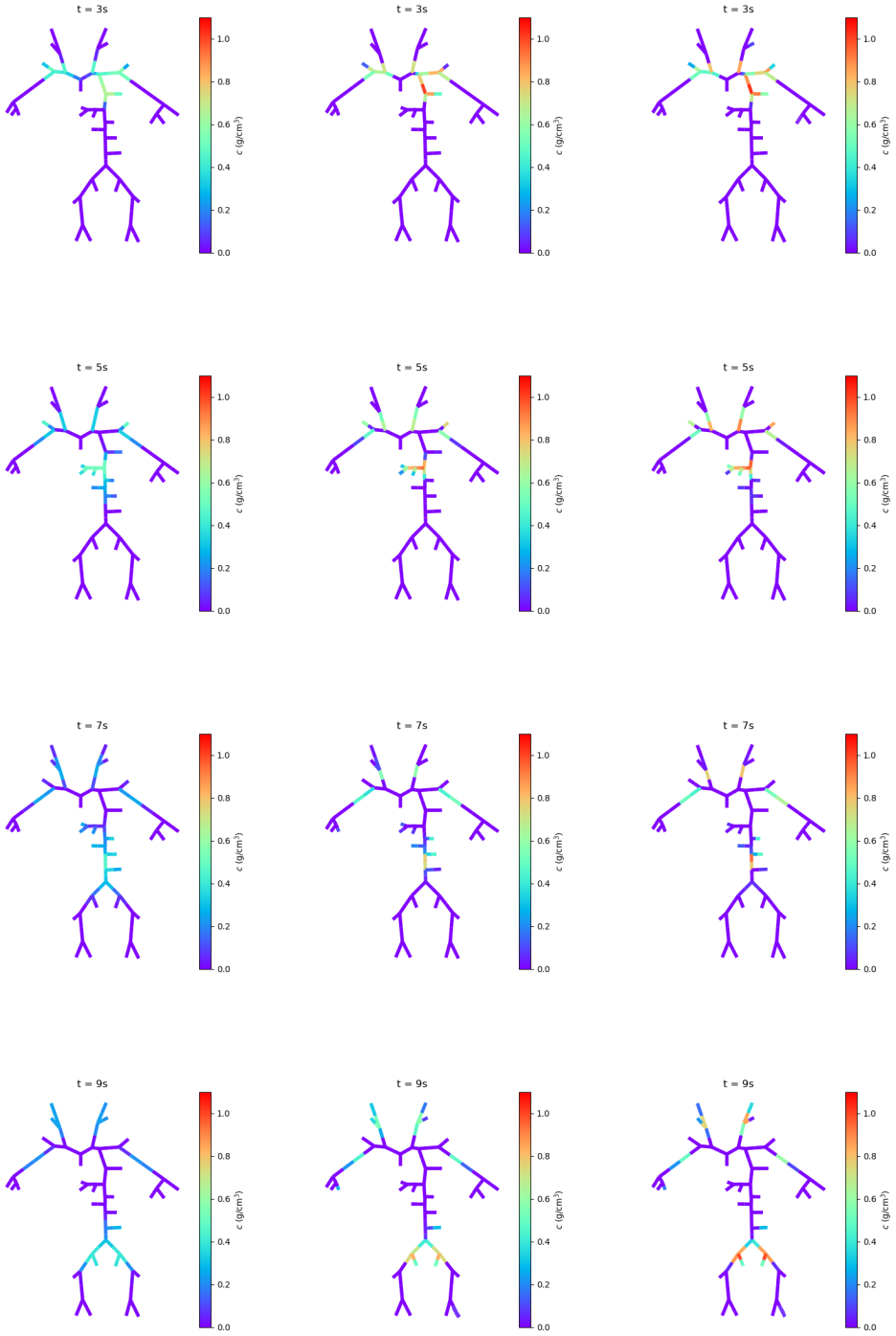

(a) $D = 2\ \mathrm{cm}^2/\mathrm{s}$ **(b)** $D = 0.2\ \mathrm{cm}^2/\mathrm{s}$ **(c)** $D = 0.02\ \mathrm{cm}^2/\mathrm{s}$

Figure 32: Visual representation of agent propagation through the arterial tree plotted at 4 times

10.3 Discussion of the model

In this final section, we provide a brief discussion of the model used in this study. We have observed that the velocity and cross-sectional area in the different arteries align closely with the existing literature. However, it is important to note that our 55-artery model represents a simplified version of the human arterial tree. We have considered an anatomically simplified system, using only the main 55 arteries while the total number of arteries in the human body is significantly higher. Also, we considered only a single type of bifurcation while realistically more complex branches exist. To further increase the model's realism more sophisticated models for the heart and capillaries could be used. In [2] they for example modeled the heart as four independent chambers and they changed the terminal coefficient to a windkessel model. Moreover, in the work of Hamel [7] a 111-artery model was used. Therefore, expanding our model to include 111 arteries and implementing more realistic models for the heart and terminal vessels would be a logical next step.

Secondly, we did not consider gravitational effects. We would expect the propagation to be affected by gravitational forces. Accounting for these aspects will further increase our understanding of the circulatory system.

There can also be made some improvement on the concentration part. Now the model is one-way, with concentration flowing out of the terminal arteries. When expanding to a two-way model, concentration can be injected at more realistic places like the arms. Remember that in this thesis we have set the diffusion coefficient to be constant in every artery. Even though this is a reasonable assumption, it is more realistic to make D artery-dependent as all the arteries do not have the same environmental properties.

Lastly, we like to address the numerical aspects of this study. For implementing the concentration we have combined a second-order upwind scheme with a central difference scheme. While these methods have provided insights into concentration propagation, they have not yielded sufficient accuracy in capturing the precise concentration wave. To that end, it might be useful to add a High-Resultion Method [6] as this increases the order of accuracy. Moreover, the numerical code can be optimized such that the computation is less heavy so a finer grid can be used. Methods such as parallelization are also useful but very difficult to implement in Python. Therefore, it might be better to use another language in further works.

11 Conclusion

In this thesis, we have investigated the behaviour of one-dimensional blood flow in the human circulatory system. To model the flow numerically, we used the Finite Volume Method in combination with the flux difference splitting approach to solving the equation governing velocity and cross-sectional area. The concentration was numerically solved by smartly switching the central difference method with a second-order upwind method.

As a test case concentration and pressure waves were considered in a normal artery. The results showed a great resemblance with the literature/analytical solution. These findings revealed that blood flow in the arterial tree propagates as a wave, with pressure traveling unhindered along the vessel while concentration gradually dilutes over time. Additionally, after the heart and boundary conditions were analysed and implemented, the blood flow of a simple 55-artery system is modeled. Again the velocity and cross-sectional area in different arteries were very comparable to the results from Sherwin et al. [1] It had moreover shown us that the solutions are composed of left and right traveling waves. In the case of no reflection at the terminal arteries, we would only expect back-traveling waves if there is a discontinuity at the bifurcation. However if we add reflection at the terminal arteries, we find that the reflected back-traveling waves interact with the forward waves creating more complex velocity waves.

Furthermore, we investigated the injection of concentration at the beginning of the model. The results demonstrated that the concentration wave advected over the arterial tree while gradually diluting. With a diffusion coefficient of $D = 0.2$ cm^2/s and a heart rate of 60 bpm, it took approximately $t = 20$ seconds for the concentration wave to reach the legs. Increasing the heart rate to 120 bpm reduced this time to approximately $t = 15$ seconds. However, it is important to note that the concentration wave dilutes during the propagation. It therefore lowers the concentration values compared to the original injection. We also observed that the diffusion coefficient significantly influenced the concentration level. For example, with $D = 0.2$ cm^2/s, the concentration at the beginning of the legs was around 70% of its original value, while increasing D by a factor of 10 reduced it to 40%. Conversely, decreasing D by a factor of 10 augmented the value to 85% of its original value.

In summary, our findings highlighted the influence of heart rate and diffusion coefficient on the propagation of concentration through the arterial tree. Advection and diffusion properties were observed, which are characteristic of concentration flow. Future research should aim to expand the model to a more realistic representation of the arterial tree by incorporating additional arteries, considering various branching points, and employing a sophisticated heart model. Additionally, improving the accuracy of concentration plots and enabling the flow of concentration in two directions within the arterial model would be valuable. The model could then be used to study the propagation of vaccines that are injected at more realistic locations.

References

[1] SJ Sherwin et al. "One-dimensional modelling of a vascular network in space-time variables". In: *Journal of engineering mathematics* 47 (2003), pp. 217–250.

[2] Jordi Alastruey Arimon. "Numerical modelling of pulse wave propagation in the cardiovascular system: development, validation and clinical applications". In: (2006).

[3] Andrey Svitenkov, Ivan Pavlov, and Sergey Chivilikhin. "A one-dimensional model of agent propagation in arterial blood flow". In: *Procedia Computer Science* 136 (2018), pp. 416–424.

[4] Johnathan P Mynard. "One-dimensional blood flow modelling with the locally conservative Galerkin (LCG) method". PhD thesis. University of Wales Swansea, 2007.

[5] Luca Formaggia and Alessandro Veneziani. "Reduced and multiscale models for the human cardiovascular system". In: *Lecture notes VKI lecture series* 7 (2003).

[6] Randall J LeVeque. *Finite volume methods for hyperbolic problems*. Vol. 31. Cambridge university press, 2002.

[7] David Hamel. "Combining MRI blood flow data with one-dimensional blood flow models to perform patient-specific noninvasive pressure prediction". In: (2020).

[8] Marco Roosendaal. "One-dimensional blood flow modelling in the human arterial system with Finite Volume Methods". In: (2017).

[9] Josef Kunes. *Dimensionless physical quantities in science and engineering*. Elsevier, 2012.

[10] C. Vuik et al. *Numerical Methods for Ordinary Differential Equations*. Vol. 2. 2015.

[11] J Peiro et al. "Numerical simulation of arterial pulse propagation using one-dimensional models". In: *Wall-fluid interactions in physiological flows* (2003), pp. 1–36.

[12] NP Smith, AJ Pullan, and Peter J Hunter. "An anatomically based model of transient coronary blood flow in the heart". In: *SIAM Journal on Applied mathematics* 62.3 (2002), pp. 990–1018.

[13] Neal L Carothers. *Real analysis*. Cambridge University Press, 2000.

[14] Sylvie Benzoni-Gavage and Denis Serre. *Multi-dimensional hyperbolic partial differential equations: First-order Systems and Applications*. OUP Oxford, 2006.

[15] "A difference method for the numerical computation of discontinuous solutions of hydrodynamic equations". In: *Math. Sbornik* 47.89 (1959), pp. 271–306.

[16] Amr G Guaily and Marcelo Epstein. "Boundary conditions for hyperbolic systems of partial differentials equations". In: *Journal of advanced research* 4.4 (2013), pp. 321–329.

[17] Guido Van Rossum and Fred L. Drake. *Python 3 Reference Manual*. Scotts Valley, CA: CreateSpace, 2009. ISBN: 1441412697.

[18] Derek S Bale et al. "A wave propagation method for conservation laws and balance laws with spatially varying flux functions". In: *SIAM Journal on Scientific Computing* 24.3 (2003), pp. 955–978.

[19] Bernardo Cockburn, George E Karniadakis, and Chi-Wang Shu. *Discontinuous Galerkin methods: theory, computation and applications*. Vol. 11. Springer Science & Business Media, 2012.

[20] Sedat Biringen. "A note on the numerical stability of the convection-diffusion equation". In: *Journal of Computational and Applied Mathematics* 7.1 (1981), pp. 17–20.

[21] Martinus Theodorus Van Genuchten. *Analytical solutions of the one-dimensional convective-dispersive solute transport equation*. 1661. US Department of Agriculture, Agricultural Research Service, 1982.

[22] Jonathan P Mynard and Joseph J Smolich. "One-dimensional haemodynamic modeling and wave dynamics in the entire adult circulation". In: *Annals of biomedical engineering* 43 (2015), pp. 1443–1460.

[23] Daniel W Lozier. "NIST digital library of mathematical functions". In: *Annals of Mathematics and Artificial Intelligence* 38 (2003), pp. 105–119.

A Appendix

All the created Python scripts can be found via this link `https://drive.google.com/drive/folders/18CnSx5ZSuHnBWSwrNZeaqPHskzHzjd7X`.

A.1 Test case tapered artery

In chapter 7 we have looked at two arterial test cases. We have seen how pressure propagates through a normal artery and what effect material variation has on this pressure wave. These test cases were compared to the work of Sherwin et al. [1] In his work, he performed one last test case which we will analyse now. A long tapered artery. This should represent a blood vessel in the middle of the arterial system. For this test case, we consider an artery where at the inlet $A_0 = 1$ cm^2. The cross-sectional area is then slowly reduced to $A_0 = 0.5$ cm^2 at the outlet. To ensure that the mass flux is constant over the artery we take the initial conditions to be $U = 1$ cm/s at the inlet and gradually increase it to $U = 2$ cm/s at the outlet. Physically we would expect c to be an order of 10 bigger than the average velocity of the blood. So we would like $c = \sqrt{\frac{\beta}{2\rho}} A_0^{\frac{1}{4}} = 10$ cm/s at the inflow. We can achieve this by assuming $\beta = 10$ and $\rho = 0.5$. Following [1] we let the artery be $L = 200$ cm running from $x = -100$ cm to $x = 100$ cm.

In the circulatory system, the velocity differs a lot from the velocity-related input at the heart. To mimic the expected velocity in an artery we take the left boundary condition to be

$$u(-100, t) = 1 - 0.4 \sin \omega t - 0.4 \sin 2\omega t - 0.2 \cos 2\omega t \tag{100}$$

Here $\omega = \frac{2\pi}{T} = \frac{2}{10}$. For the right boundary, we again take a periodic condition so

$$s_2(100, t) = s_2(100, 0) \tag{101}$$

A.1.1 Implementation boundary conditions

Analogously as done in chapter 7 we derive a numerical scheme to implement the boundary conditions. We first note that the right boundary can be implemented easily as it is already defined in terms of the characteristic variables. For the left boundary, we have to do some extra work. We again remember eqn (28) and derive at

$$s_1(-100, t) = 2u(-100, t) - s_2(-100, 0) \tag{102}$$

As said in the forward boundary condition section, the left boundary s_2 is fixed at its initial state.

A.1.2 Results of the tapered artery

We subdivide the domain into $n = 400$ intervals. Below in figure 34 the comparison with the literature is made.

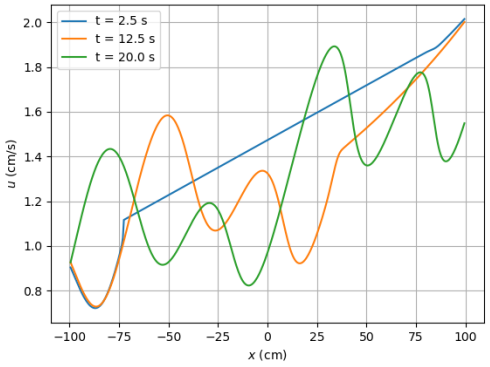

(a) Velocity of the tapered artery test case in our model

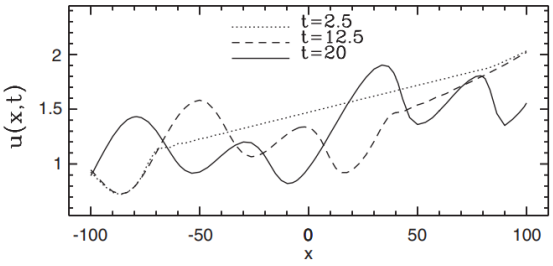

(b) Velocity of the tapered artery test case from Sherwin et al. [1]

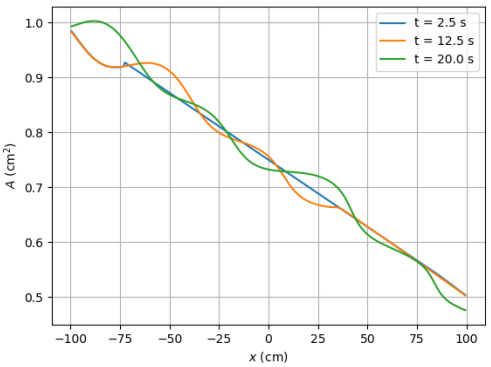

(a) Cross-sectional area of the tapered artery in our model

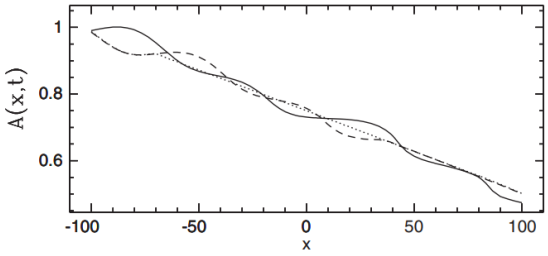

(b) Cross-sectional area of the tapered artery from Sherwin et al. [1]

Figure 34: Results of the test case of the tapered artery. The cross-sectional area in the artery is plotted at $t = 2.5$s, $t = 12.5$s, and $t = 20$s in the lower row and the velocity in the upper row. In the left column, our results are depicted and in the right column, the results from [1].

First of all, we note that again our model is very comparable to the literature. Both plots of figure 34 are almost identical to the work of Sherwin. In addition, it is more interesting to look at the bevaviour of the solution. We notice that the velocity is fluctuating over a linearly increasing line. This line goes from $U = 1$ cm/s to $U = 2$ cm/s, which is exactly our initial condition. When looking at the velocity in the figure we recognize a repeating part. This is best visible in the $t = 0$ plot between $x = -100$ and $x = 0$. We can see, this is in fact the boundary condition. Figure 35 shows this boundary condition.

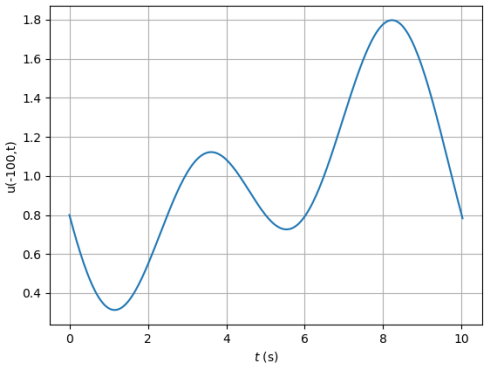

Figure 35: The inflow boundary condition $u(-100, t)$

The inflow boundary condition has a period of $T = 10$s. So this explains why we recognize the inflow function to be repeated twice in the $t = 20$ plot in figure 34. Moreover, it is interesting to note that the wave speed is gradually decreasing. Since $c_0 = \sqrt{\frac{\beta}{2\rho}} A_0^{\frac{1}{4}}$ with A_0 decreasing over length, c_0 decreases too. This influences the velocity of the waves as $\lambda = U + c$. Inevitably, this would imply that a bit more than two periods should be visible in the plot. However, this effect is very small and therefore barely visible in the plots. Lastly, we want to mention that this test case is not physical. In the circulatory system, there would not exist a vessel of 2m without any bifurcations.

A.2 Analysis of the different methods for solving the advection-diffusion equation

When numerically solving the advection-diffusion equation we could have chosen between different integration and discretization methods. We have used the finite volume method to solve the velocity and cross-sectional change in the arteries. It would therefore seem elegant to also use finite volume for solving the concentration. But let us analyse the difference between two of these methods in more detail. For the advection term, we will compare the central difference scheme presented in eqn (77) with a second-order upwind scheme. For that, we follow LeVeque [6] and use the second-order stable *Beam-Warming Method* (BWM). The advection term is then written as

$$c_i^{n+1} = c_i^n - U_i^n \frac{\Delta t}{2\Delta x}(3c_i^n - 4c_{i-1}^n + c_{i-2}^n) + \frac{1}{2}\left(\frac{U_i^n \Delta t}{\Delta x}\right)^2 (c_i^n - 2c_{i-1}^n + c_{i-2}^n) \tag{103}$$

Figure 36 shows the comparison between the two in the test case from chapter 8. In the figure, we can see that both generate very similar results which are also similar to the analytical solution. Looking more closely, the solution with the Beam-Warming method seems to generate a slightly more accurate result. However, the computation power of this method is higher than that of the central difference method. Moreover, the difference between the two is so small it does not hinder us when working with central differences. In general, both two methods generate the same results. However, we must be careful when using central difference when diffusion plays a role. It had been shown that when the Péclet number exceeds 2, the central difference approach will generate spurious oscillations. These oscillations can be greatly reduced by using an upwind method like the BWM. On the other hand, if the Péclet number is far below 2 the central difference is in general more accurate. To summarize, we can use both the Beam-Warming method as the central difference method to solve the advection-diffusion equation but in solving

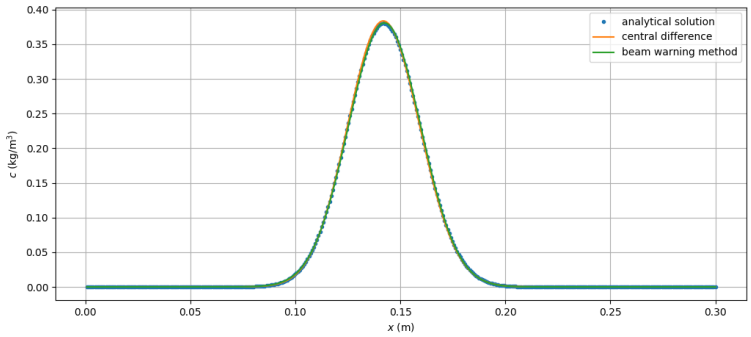

Figure 36: The solution of the numerical test case as described in chapter 8. The solution computed with the Beam-Warming Method and with the central difference method are plotted. The dots represent the analytical solution. All the plots show the concentration $c(x,t)$ at $t = 0.3$s.

such we must remember the Péclet number. Later in the work, we will actually use a combination of the two to achieve an optimal stable result.

A.3 Test case concentration 2

In chapter 8 we have looked at a test case of an artery. There we have considered blood that is flowing with a constant velocity. However, in the final arterial system, the velocity is not constant. For that reason, we will now analyse a test case in with a variable velocity. We consider an artery at which a periodic pressure wave is applied. This pressure wave results in the contraction and release of the artery at $x = 0$. We use this kind of periodic pressure wave as this mimics the behaviour of the heart. Figure 37 shows the boundary pressure.

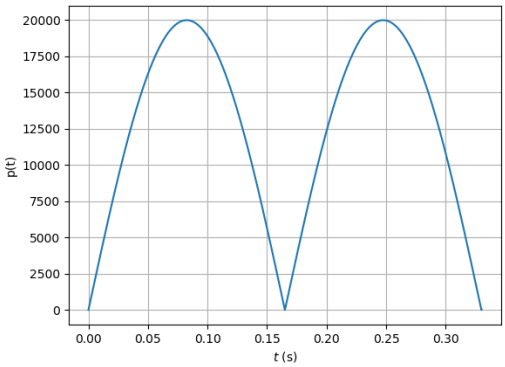

Figure 37: A plot of the pressure at the inflow boundary

Note that we have given the pressure wave quite a large amplitude, this is because it will generate higher velocities of the blood. Therefore, the advection property can better be seen. Moreover, we once again inject a chemical species with a concentration of $c_0 = 1$ kg/cm^3 at the beginning of the artery

during a period of $t_0 = 0.033$ s. We take $D = 1$ cm^2/s and all the other parameters of importance are chosen similar to the normal artery test case from chapter 7. The numerical results of the concentration propagation are shown in figure 38.

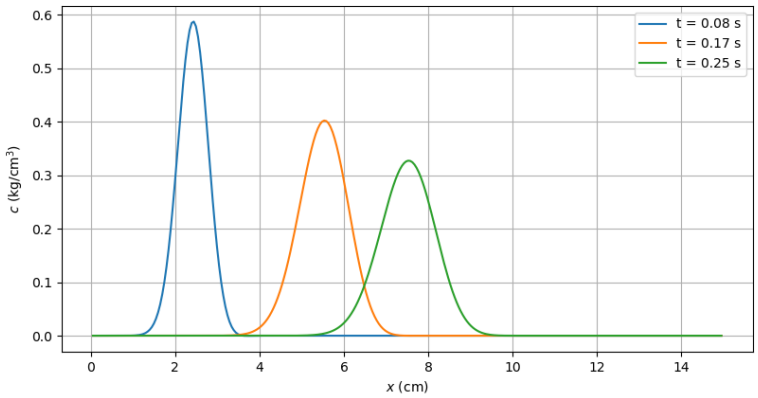

Figure 38: The numerical solution of the concentration propagation in a normal artery with changing velocity. The concentration profile is plotted at three time points, $t = 0.08$s, $t = 0.17$s, and $t = 0.25$s.

Looking at figure 38 we again clearly recognize the advective and diffusive characteristics of the concentration profile. Note that we have the same shape as in our previous test case in chapter 8. However, there is an important difference. Let us consider the distances each wave has traveled during the three times. We note that during the first 0.08 s the wave has traveled around the 2.5 cm, in the next 0.08 s the wave has traveled around the 3.0 cm, and in the following 0.08 s the wave has only traveled 2.0 cm. We thus see that the distances over which the wave propagates, differ over time. This is exactly the effect of a variable velocity. In figure 10 the wave propagated each time the same distance only because the velocity was constant. Lastly, we want to say something about the correctness of the solution. Unfortunately, our specific test case has no analytic solution so we cannot compare it that way. For that reason, we will perform two alternative numerical tests to assess the reliability of the solution. First of all, we use the method comparison test. Originally we solved the concentration profile using finite difference. For this test, we solve eqn. (16) using a second-order upwind scheme. A similar result in both cases gives us confidence about the numerical solution. Secondly, we do a grid analysis. In this test, we will systematically increase and decrease the grid. If the solution is independent of the grid size, then the confidence in our solution grows. In figure 39 the computed solution together with these two alternative tests are shown.

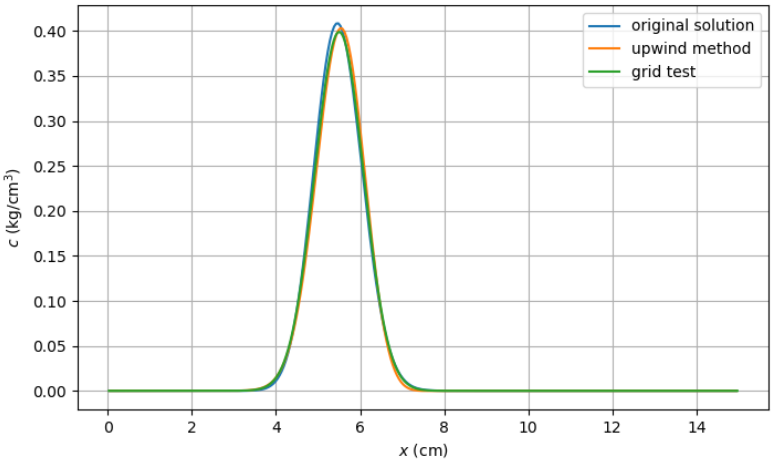

Figure 39: A plot of the original computed concentration solution together with the two alternative tests. The plot shows the original solution as seen in figure 38, the solution of the test case when the grid size is doubled, and the solution of the test case when a second-order upwind scheme is used. In all these three plots $c(x,t)$ is shown with $t = 0.17$s.

In figure 39 we can see that all the tests generate very similar results. There are some small deviations between the three. The difference between the original solution and the grid test can for example be partly explained by the fact that even though the x-domain is doubled in size, the t-domain is not exactly doubled. This is due to the fact that in the code Δt is determined each time step to ensure that the CFL condition is satisfied. Altogether, these tests have given us more confidence in our numerically computed solution besides the small anomalies.

A.4 Physiological data from the 55 arteries

The physiological data from the 55 arteries we use in our model from Sherwin et al. [1]

Table 1: Physiological data of the 55 arteries

#	Artery	Length (cm)	Area (cm^2)	β($kg\,s^{-2}\,cm^{-2}$)	R_t
1	Ascending Aorta	4.0	5.983	97	—
2	Aortic Arch I	2.0	5.147	87	—
3	Brachiocephalic	3.4	1.219	233	—
4	R. Subclavian I	3.4	0.562	423	—
5	R. Carotid	17.7	0.432	516	—
6	R. Vertebral	14.8	0.123	2590	0.906
7	R. Subclavian II	42.2	0.510	466	—
8	R. Radial	23.5	0.106	2866	0.82
9	R. Ulnar I	6.7	0.145	2246	—
10	R. Interosseous	7.9	0.031	12894	0.956
11	R. Ulnar II	17.1	0.133	2446	0.893
12	R. Internal Carotid	17.6	0.121	2644	0.784
13	R. External Carotid	17.7	0.121	2467	0.79
14	Aortic Arch II	3.9	3.142	130	—
15	L. Carotid	20.8	0.430	519	—
16	L. Internal Carotid	17.6	0.121	2644	0.784
17	L. External Carotid	17.7	0.121	2467	0.791
18	Thoracic Aorta I	5.2	3.142	124	—
19	L. Subclavian I	3.4	0.562	416	—
20	Vertebral	14.8	0.123	2590	0.906
21	L. Subclavian II	42.2	0.510	466	—
22	L. Radial	23.5	0.106	2866	0.821
23	L. Ulnar I	6.7	0.145	2246	—
24	L. Interosseous	7.9	0.031	12894	0.956
25	L. Ulnar II	17.1	0.133	2446	0.893
26	Intercostals	8.0	0.196	885	0.627
27	Thoracic Aorta II	10.4	3.017	117	—
28	Abdominal I	5.3	1.911	167	—
29	Celiac I	2.0	0.478	475	—
30	Celiac II	1.0	0.126	1805	—
31	Hepatic	6.6	0.152	1142	0.925
32	Gastric	7.1	0.102	1567	0.921
33	Splenic	6.3	0.238	806	0.93
34	Superior Mesenteric	5.9	0.430	569	0.934
35	Abdominal II	1.0	1.247	227	—
36	L. Renal	3.2	0.332	566	0.861
37	Abdominal III	1.0	1.021	278	—
38	R. Renal	3.2	0.159	1181	0.861
39	Abdominal IV	10.6	0.697	381	—
40	Inferior Mesenteric	5.0	0.080	1895	0.918
41	Abdominal V	1.0	0.578	399	—
42	R. Common Iliac	5.9	0.328	649	—
43	L. Common Iliac	5.8	0.328	649	—
44	L. External iliac	14.4	0.252	1493	—
45	L. Internal Iliac	5.0	0.181	3134	0.925
46	L. Femoral	44.3	0.139	2559	—
47	L. Deep Femoral	12.6	0.126	2652	0.885
48	L. Posterior Tibial	32.1	0.110	5808	0.724
49	L. Anterior Tibial	34.3	0.060	9243	0.716

#	Artery	Length (cm)	Area (cm^2)	β ($kg\,s^{-2}\,cm^{-2}$)	R_t
50	R. External Iliac	14.5	0.252	1493	—
51	R. Internal Iliac	5.1	0.181	3134	0.925
52	R. Femoral	44.4	0.139	2559	—
53	R. Deep Femoral	12.7	0.126	2652	0.888
54	L. Posterior Tibial	32.2	0.110	5808	0.724
55	R. Anterior Tibial	34.4	0.060	9243	0.716

A.5 Friction and reflection

In the models we have analysed before, we have neglected the frictional forces and we did not include reflection at the terminal arteries. In this section, we analyse the behaviour of the blood when friction and reflection are added. For the 55-artery model we consider, the value of R_t has been experimentally determined. Moreover, we implement eqn (68) in our code. We wave taken $\zeta = 9$, $\nu = 0.026$ cm^2/s according to the literature [3]. Below the results are shown and compared to [1]. Note that in their work they did not include any frictional terms but only reflection at the terminal arteries. But because the friction is relatively low, comparing is still relevant. Below the results are shown of artery 1 and artery 49.

We first note that again our model is in agreement with the literature. All the plots show very much resemblance with the results from Sherwin et al. However, when looking more closely we do see some differences between the two. In artery 49, the velocity at some time points is lower than in the literature. This is also visible in the other 3 plots of artery 49. These differences are probably due to the addition of a friction force in our model. The frictional term slightly lowers the velocity as it works as a resistance. The difference is of course also explained by the different methods used. In addition, including terminal reflection increases the number of waves in the system. This is because of the additional back-traveling waves. The forward waves get reflected generating back-traveling waves, which in their turn interact with other forward waves creating a complex pattern. This is for example visible in the s_2 plot of artery 49. Instead of no s_2-wave a complex wave is now generated. Note that the inclusion of friction and reflection creates more differences in the waves between the arteries. In figures 16 and 17 the velocity waves look similar but shifted and changed in value. In the new model with reflection, we see that there is a clear difference in shape between the waves in artery 1 and 49. Especially artery 49 now has a more complex pattern. Lastly, we want to discuss a physical phenomenon that can be seen in the results. In the area plot of artery 1, we notice a small dip around $t = 9.3$s. This indentation is called a *diacrotic notch*. A diacrotic notch appears as a small dip that occurs shortly after the peak of the systolic phase. It is followed by a secondary rise before the waveform descends during the diastolic phase. This is exactly what we see. The area is increasing during the first seconds and then slowly descends. Physically, the diacrotic notch is caused by the closure of the aortic valve and the resulting brief interruption in the arterial blood flow. It is a nice detail that it is also returning in our results.

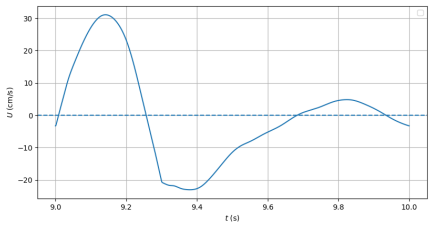

(a) The velocity in artery 1 with our model

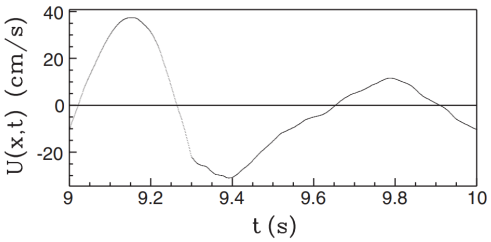

(b) The velocity in artery 1 from [1]

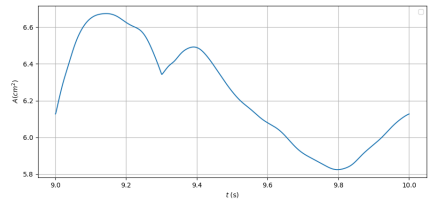

(c) The cross-sectional area in artery 1 with our model

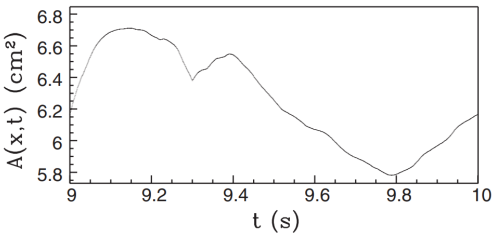

(d) The cross-sectional area in artery 1 from [1]

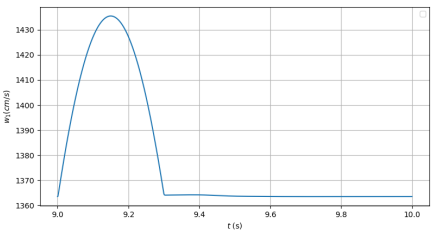

(e) The characteristic variable s_1 with our model

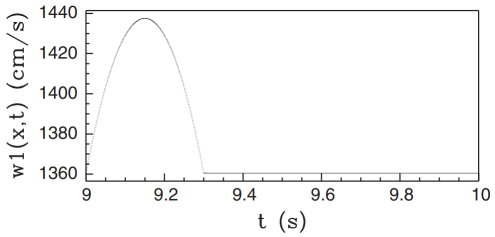

(f) The characteristic variable s_1 from [1]

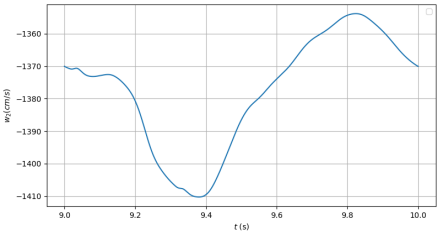

(g) The characteristic variable s_2

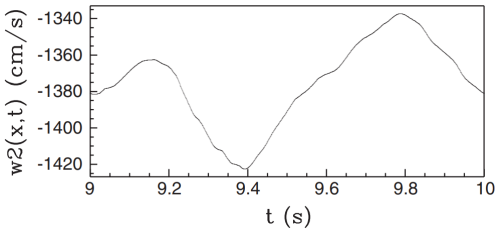

(h) The characteristic variable s_2 from [1]

Figure 40: The results of artery 1 of our model (including reflection and friction) together with the literature results from [1]. From top to bottom, the velocity, cross-sectional area, and characteristic variables s_1 and s_2 are plotted respectively. The left column is our results and the right column is from [1].

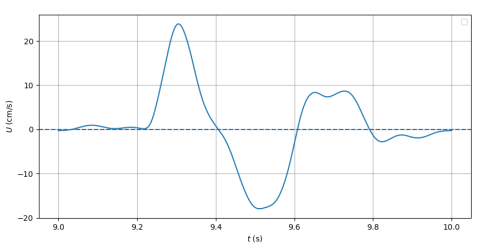

(a) The velocity in artery 49 with our model

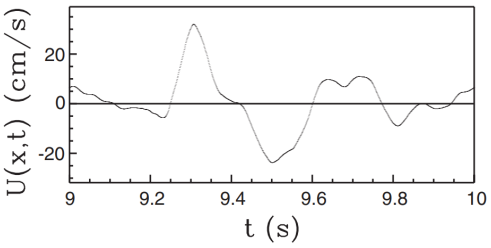

(b) The velocity in artery 49 from [1]

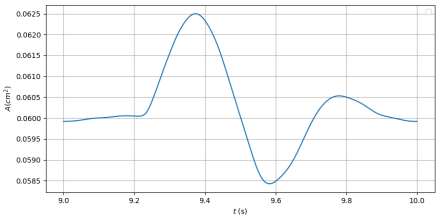

(c) The cross-sectional area in artery 49 with our model

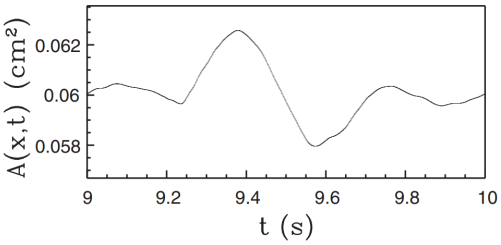

(d) The cross-sectional area in artery 49 from [1]

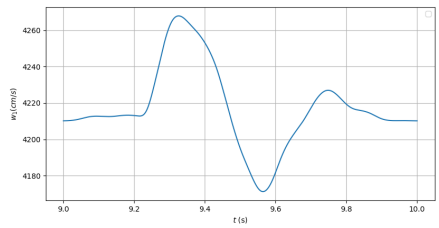

(e) The characteristic variable s_1 with our model

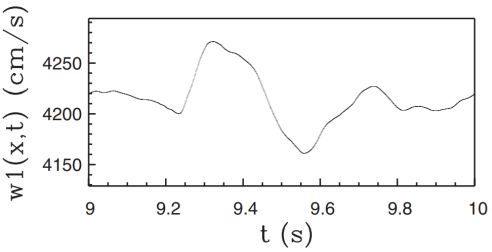

(f) The characteristic variable s_1 from [1]

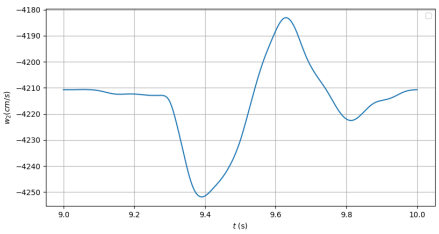

(g) The characteristic variable s_2

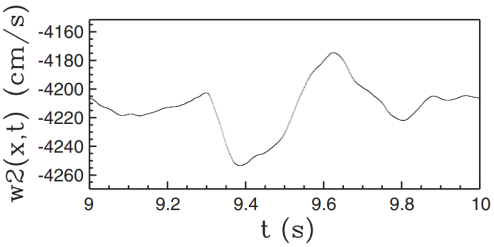

(h) The characteristic variable s_2 from [1]

Figure 41: The results of artery 49 of our model (including reflection and friction) together with the literature results from [1]. From top to bottom, the velocity, cross-sectional area, and characteristic variables s_1 and s_2 are plotted respectively. The left column is our results and the right column is from [1].